

Distribution and stoichiometry of Al, Mn, Fe, Co, Ni, Cu, Zn, Cd, and Pb in the East China Sea

Yuzuru Nakaguchi¹, Yoshinori Ikeda², Atsushi Sakamoto², Zheng Linjie³, Tomoharu Minami⁴, Yoshiki Sohrin³

¹School of Science and Engineering, Kindai University, 3-4-1 Kowakae, Higashiosaka, Osaka, 577-8502, Japan (*Correspondence: nakaguch@chem.kindai.ac.jp, TEL:+81-6-4307-3409, FAX:+81-6-6723-2721)

²Graduate School of Science and Engineering, Kindai University, 3-4-1 Kowakae, Higashiosaka, Osaka, 577-8502, Japan

³Institute for Chemical Research, Kyoto University, Uji, Kyoto, 611-0011, Japan

⁴Engineering and Technology Department, Kanazawa University, Kanazawa, Ishikawa 920-1192, Japan

Abstract

The dissolved (d) and total dissolvable (td) trace metals were determined in sea water samples collected from the East China Sea (ECS). Labile particulate (lp) species was calculated as td minus d, and the sectional and vertical distributions of d and lp trace metals were evaluated. The surface concentrations of dAl, dCo, dNi, dCu, and dPb were higher in the continental shelf region than in the Kuroshio region. lpAl and lpFe were the dominant species below a depth of 400 m, and a strong positive correlation was observed between them in the Kuroshio region. The enrichment factor (*EF*) against crustal abundance was calculated for the purpose of estimating the origin of dMs in the ECS. The *EF*(dFe) was close to unity. These results suggest that both lpFe and dFe are dominated by crustal sources. The other elements had high *EF*, indicating significant contributions from other sources. *EF*(dPb) was close to the enrichment factor in aerosol, suggesting atmospheric input from anthropogenic sources. The dM/P ratios were calculated to investigate the validity of the extended Redfield ratio in the ECS. The Mn/P, Co/P, Cu/P, Zn/P, and Cd/P ratios in shallow water (<200 m) were within the same order of magnitude as those in phytoplankton. In contrast, the Al/P and Fe/P ratios were, respectively, 27 and 213 times higher in phytoplankton compared to those in shallow water. These results suggest that dFe is a potential limiting factor for biological production, although it is not exhausted in surface water.

Keywords GEOTRACES, East China Sea, Trace metals, Total dissolvable species, Dissolved species, Labile particulate species

1 Introduction

The East China Sea (ECS) is a marginal sea bounded by China, Taiwan, Korea, and Japan. The ECS contains a broad continental shelf, and a major western boundary current, the Kuroshio, travels along the outer edge of that shelf (Ichikawa and Beardsley 2002). The shelf region shallower than 200 m occupies approximately 70 % of the area of the ECS and the Yellow Sea. The volume of water on the shelf is $4.5 \times 10^4 \text{ km}^3$. The Okinawa Trough lies in the southern and eastern ECS, where the maximum water depth is greater than 2000 m in its southern section and less than 1000 m in its northeastern section. Two of China's largest rivers, the Changjiang (Yangtze River) and the Huanghe (Yellow River), supply freshwater to the ECS. The Changjiang is the single most important freshwater source in the ECS; approximately $30.0 \times 10^3 \text{ m}^3/\text{s}$ of freshwater discharges from the Changjiang to the ECS (Beardsley et al. 1985; Chen et al. 1994). A large amount of inorganic nitrogen and particulate organic carbon annually enters the ECS (Dagg et al. 2004; Liu et al. 2003). In addition, the Kuroshio subsurface waters upwell onto the ECS shelf, providing a large amount of nutrients (Chen 1996). The mean residence time for the shelf water is estimated to be approximately 2.3 y based on measurements of $^{228}\text{Ra}/^{226}\text{Ra}$ (Nozaki et al. 1989).

Some bioactive trace metals, such as Fe, Mn, Co, Cu, Ni, Zn, and Cd are thought to play a key role in controlling oceanic biogeochemical processes (Morel et al. 2003; Morel and Price 2003). The distribution of dissolved Fe (dFe) in the open ocean has been extensively studied to prove the importance of dFe in limiting biological productivity (Landing and Bruland 1987; Martin and Gordon 1988; Martin et al. 1989; Wu and Luther 1994; Bruland et al. 1994; Zheng and Sohrin 2019). Some studies suggest that over 99 % of dFe is strongly complexed by organic Fe-binding ligands (Gledhill and van den Berg 1994; Rue and Bruland 1995; Wu and Luther 1995; Öztürk et al. 2003; Ibanmami et al. 2011; Kondo et al. 2012). Dissolved Mn in the open ocean has a scavenging profile (Statham et al. 1998; Middag et al. 2011; Wu et al. 2014; Zheng et al. 2019). It has been attributed to a source of eolian dust deposition of Mn to the surface ocean and a sink via Mn(II) oxidation by dissolved oxygen in seawater (Klinkhammer and Bender 1980; Landing and Bruland 1980,1987). There are some similarities between the distributions of dCo and dMn (Martin et al. 1990; Fitwater. et al. 2000; Saito and Moffet 2002; Ezo et al. 2004; Saito et al. 2004; Bown et al. 2011). The low solubility of Co in seawater is

partly derived from the oxidation of Co(II) to Co(III); oxidation can be achieved on Mn oxides by Mn-oxidizing bacteria (Tebo et al. 1984; Tebo 1998). Co is clearly used by phytoplankton as a micronutrient in culture studies, and dCo shows a linear correlation with phosphate in the upper ocean (Sunda and Huntsman 1995; Saito et al. 2002; Zheng et al. 2019). Although Cu is an essential micronutrient for marine phytoplankton (Peers and Price 2006; Maldonado et al. 2006), the depth profiles of dCu do not resemble those of macronutrients and instead display a monotonic increase with depth (Boyle and Edmond 1975; Boyle et al. 1977; Bruland 1980; Ezoe et al. 2004; Boye et al. 2012; Thompson et al. 2014; Heller and Croot 2015; Roshan and Wu 2015; Zheng et al. 2017). The modest vertical gradient more likely results from remineralization of Cu during early diagenesis in sediments, leading to a flux from pore waters to overlying waters (Boyle et al. 1977). Dissolved Ni is never fully depleted in the surface ocean and dNi is not generally considered to be a limiting factor (Middag et al. 2020). Recent studies, however, report that Ni is required for the growth of phytoplankton and cyanobacteria (Ho 2013). Dissolved Zn shows a stronger correlation with silicate than with phosphate in the ocean (Bruland 1980; Janssen and Cullen 2015; Kim et al. 2017; Wang et al. 2019). This is a paradox because organisms usually incorporate Zn into soft tissue for metabolism (Ellwood and Hunter 2000). Dissolved Cd in the open ocean exhibits genuine nutrient-type behavior and a linear relationship with phosphate (Boyle 1988; Bruland 1980; Bruland and Franks 1983; Danielson et al. 1985; Sakamoto-Arnold et al. 1987; Hunter and Ho 1991; Nolting and de Baar 1994; Fitzwater 2000; Abe 2002; Cid et al. 2011; Xie et al. 2015; Hernandez-Candelario et al. 2019).

In addition, Al and Pb are key elements in marine geochemistry (**SCOR Working Group 2007**). The oceanic distribution of dAl is primarily controlled by terrigenous sources, rapid scavenging from a water column, and internal cycling (Hydes 1983; Measures et al. 1986; Orians and Bruland 1986; Hydes et al. 1988; Measures and Edmond 1988; Hall and Measures 1998; Measures and Vink 1999; Kramer et al. 2004; Obata et al. 2004; Zheng et al. 2019). Fluvial input has been suggested as an important source of dAl in coastal regions (Morris et al. 1986; Brown et al. 2010). Orians and Bruland (1986) suggested that dAl can be scavenged by biogenic particles in high-productivity surface waters with high export production. Gehlen et al. (2002) suggested that Al can also be removed from seawater as it is incorporated into diatoms during silica frustule biosynthesis. Dissolved Pb in the ocean exhibits scavenged-type behavior, which is primarily due to the atmospheric supply from anthropogenic sources and the adsorption of dPb on particles in seawater (Wu and Boyle 1997; Windom et al. 1985; Kraepiel et al. 1997; Ezoe et al. 2004; Zheng et al. 2019).

There are some reports on the distributions of dissolved trace metals in the ECS for Al (Ren et al. 2006), Mn (Wang et al. 2016), Fe (Su et al. 2015; Yang et al. 2017; Sasayama et al. 2018), Cd (Hsu et al. 2003B), and Pb (Lin et al. 2000; Li et al. 2014). The distribution of dAl in the ECS and the Yellow Sea was reported by Ren et al. (2006). The distribution of dAl in the Yellow Sea shows the effect of land-source input from adjacent rivers and the Changjiang with obvious seasonal variations. On the other hand, 250 km from the Changjiang mouth, the freshwater input is hardly detected and the incursion of Kuroshio waters becomes dominant (Ren et al. 2006). Su et al. (2015) reported the vertical distribution of dFe in the coastal waters of the ECS. High dFe concentrations were observed at estuary stations, whereas low concentrations were observed at offshore stations. They suggested that dFe at estuary stations is mainly influenced by the input of the Changjiang. The concentrations of dPb in the upper water in the southern ECS are several times higher than those in the Pacific, corresponding to much higher atmospheric supplies of Pb to the ECS (Lin et al. 2000). Seasonal variability of dPb was observed in the coastal waters of the ECS (Li et al. 2014). They suggested that riverine and atmospheric inputs are the main sources of dPb in spring in this area. Thus, although there are several research reports on the bioactive trace metals in the ECS, the large-scale distributions and stoichiometry of trace metals in the ECS are not well understood.

We have developed a multielemental determination method for Al, Mn, Fe, Co, Ni, Cu, Zn, Cd, and Pb in seawater samples by solid-phase extraction with inductively coupled plasma mass spectrometry (Minami et al. 2015; Sohrin et al. 2008). Using this method, we have elucidated the distributions and stoichiometry of the trace metals in the Indian Ocean (Vu and Sohrin 2013), the Bering Sea (Cid et al. 2011), the Chukchi and Beaufort Seas (Cid et al. 2012), and the North Pacific Ocean (Zheng et al. 2019; Zheng et al. submitted; Zheng et al. 2017; Zheng and Sohrin 2019). In this study, seawater was sampled at stations in the ECS and the adjacent Kuroshio region, as part of the Japanese GEOTRACES program. We measured dissolved (d) and total dissolvable (td) concentrations of the nine trace metals using filtered and unfiltered seawater, respectively, and obtained labile particulate (lp) concentrations which were calculated as td minus d. As far as we know, this is the first systematic and comprehensive study of the key trace metals in seawater in the ECS.

2 Study Area

Seawater samples were collected during the KH-15-3 cruise of R/V Hakuho Maru of the Japan Agency for Marine-Earth Science and Technology (JAMSTEC) from October 14

to November 2, 2015. The sampling locations are shown in Fig. 1. Station AND 22 (123.00E, 25.17N; 1671 m) is located in the southwestern ECS, which is the closest station to Taiwan Island. Station AND 26 (126.08E, 28.95N; 105 m) is located in the continental shelf region of the ECS. Stations AND 6 (129.10E, 29.65N; depth 826 m) and AND 31 (127.14E, 28.30N; 965 m) are located in the northeastern ECS, and station AND 34 (130.75E, 29.37N; 2987 m) is located above the continental slope in the North Pacific Ocean.

The potential temperature-salinity (TS) diagram for the five stations is presented in Fig. 2. The Kuroshio enters the ECS through the channel between Taiwan Island and the Yonagunijima Archipelago (Nitani 1972; Johns et al. 1995). In the ECS, the Kuroshio then flows northeastward along the continental shelf break to 30°N. The flow on the left of the Kuroshio separates into the Tsushima Current (Sverdrup et al. 1942). Our T-S diagrams show that the four sampling stations (AND 6, AND 22, AND 31, and AND 34) are within the same current system, that is, Kuroshio. The T-S diagram of Station AND 26 differs from that of the other four stations. The relatively high temperature and low salinity ($S = 33.96\text{--}34.68$) of the surface water is thought to be Changjiang Diluted Water (CDW) (Chang and Isobe 2003).

3 Methods

3.1 Sampling

Seawater samples were collected using a Carousel system (SBE-32, Sea-Bird Scientific, Bellevue, Washington, USA) with a conductivity, temperature, and depth sensor (CTD; Model SBE-9-plus, Sea-Bird Scientific, Bellevue, Washington, USA). The insides of Niskin-X bottles were coated with Teflon and cleaned with 1 % detergent, 0.1 M hydrochloric acid, and deionized water (MQW) prepared using a Milli-Q system (Merck Millipore, Darmstadt, Germany).

All seawater samples were transferred from clean Niskin-X bottles to precleaned, 250-mL low-density polyethylene Nalgene bottles (Thermo Fisher Scientific, Waltham, MA, USA) in a clean bubble. Unfiltered samples were collected from the clean Niskin bottles directly to determine total dissolvable trace metals (tdMs), and filtered samples were passed through an AcroPak capsule filter with a pore size of 0.2 μm (Pall, Port Washington, New York, USA) to determine dissolved trace metals (dMs). Immediately after collection, HCl (Tamapure AA-10, Tama Chemicals, Kawasaki, Japan) was added to both the unfiltered and filtered seawater samples to achieve a final HCl concentration

of 0.010 mol/kg (pH ~ 2.2). The samples were stored at room temperature for approximately two years until analysis. Although the pH was slightly higher than the 1.8 recommended by GEOTRACES and UV irradiation was not applied, the storage time was fairly long.

The samples for salinity, nutrient, and Chl *a* analysis were obtained using normal Niskin-X bottles that were not acid-cleaned.

3.2 Analysis

An off-line pre-concentration procedure was reported previously (Minami et al. 2015; Sohrin et al. 2008). An improved commercially available solid-phase extraction apparatus SPE-100 (Hiranuma Sangyo) was used for the preconcentration of trace metals in seawater, which was conducted using a chelating resin with ethylenediaminetriacetic and iminodiacetic acid groups (NOBIAS CHELATE-PA1, Hitachi High-Technology). **A td sample was passed through an inline filter, when it is processed using a SPE-100.** A high-resolution inductively coupled plasma mass spectrometer (HR-ICP-MS), equipped with a magnetic sector mass spectrometer (ELEMENT 2, ThermoFisher), was used to determine the concentrations of dM and tdM in seawater. The studied isotopes were ²⁷Al, ⁵⁵Mn, ⁵⁶Fe, ⁵⁹Co, ⁶⁰Ni, ⁶³Cu, ⁶⁶Zn, ¹¹⁴Cd, and ²⁰⁸Pb. Calibration lines for the trace metals were obtained using standard solutions containing 1 M HNO₃ (TAMAPURE AA-10). The standard solutions were measured at appropriate intervals during analysis to correct changes in the background and in sensitivity. We evaluated procedure blanks using MQW as a sample. The MQW was initially acidified with HCl and then adjusted to pH 6.0 for preconcentration in a similar manner to the seawater samples. The concentrations of labile particulate metals (lpMs) were obtained from the difference between tdMs and dMs. The lp species include (1) metal oxides, hydroxides, sulfides, and carbonates, (2) metal ions adsorbed on mineral surfaces, (3) metal ions complexed with organic matter in suspended particles (Ezoe et al. 2004), and (4) metal ions dissolved from aluminosilicate minerals (Zheng et al. 2019).

No significant difference in procedure blank for dMs and tdMs were observed, and we defined the detection limits for dMs and tdMs as three times the standard deviation (sd) of the procedure blank. The concentrations of lpMs were determined by the difference between tdMs and dMs. Because the relative standard deviation (rsd) was ~5% for both tdMs and dMs, the detection limits of lpMs were defined using the following equation considering the propagation of uncertainty: $2 \times \sqrt{2} \times 0.05 \times C_{ave}$, where C_{ave} represents the average concentration of dMs in this study. The procedure blanks and

detection limits are summarized in Table S1 (online supplementary material). We measured the GEOTRACES open-ocean reference samples SAFe-D2, GS, and GD at an early point in the study (Minami et al. 2015). We measured certified reference materials for trace metals, CASS-4 (National Research Council of Canada) at a midpoint in this study. The analytical results of the seawater reference material are shown in Table S2 (online supplementary material). The concentration of each element in this study was within $\text{ave} \pm 2\text{sd}$ of the certified value.

The temperature was measured by the CTD. Salinity and nutrients (NO_3 , NO_2 , PO_4 , and $\text{Si}(\text{OH})_4$) were, respectively, measured on board using a salinometer (Autosal 8400B, Ocean Scientific International Ltd., Havant, UK) and an autoanalyzer (SWATT, BLTEC, Osaka, Japan). Nutrient data were checked using a certified reference material for seawater analysis (KANSO Co. Ltd., Japan). The Ocean Data View software package was used to analyze the data and prepare figures (Schlitzer 2015).

4 Results

4.1 Hydrography, dissolved oxygen, nutrients, and Chl a.

The seawater data are summarized in Table S3 (online supplementary material). The full-depth vertical profiles of potential density anomaly (σ_θ), potential temperature (θ), salinity, dissolved oxygen, nitrate, nitrite, phosphorous, and silicic acid are shown in Fig. 3. The sectional distributions of potential temperature, salinity, dissolved oxygen, nitrate, nitrite, phosphorous, and silicic acid from the surface to a depth of 1500 m between stations AND 26 and AND 34 are shown in Fig. 4. At the shelf station AND 26, dissolved oxygen decreased in bottom water, where nitrate, nitrite, phosphorous, and silicic acid significantly increased. A maximum of nitrite occurred around a depth of 100 m between AND 26 and AND 06, suggesting nitrate reduction on the shelf bottom and in the water column in the ECS.

4.2 AI

The full-depth vertical profiles of dAI and lpAI are shown in Figs. 5(A) and 7(A), respectively. The sectional distributions of dAI and lpAI from the surface to a depth of 1500 m between AND 26 and AND 34 are shown in Figs. 6(A) and 8(A), respectively. The concentration ranges for dAI and lpAI at AND 26, in the continental shelf region, were 18.6–23.7 and 12.7–2872 nmol/kg, respectively, which were substantially higher

than those at the other stations, suggesting terrigenous input. These concentrations are comparable with those observed in the southern Yellow Sea (Ren et al. 2006). Both dAl and lpAl dropped sharply within 130 km from AND 26 to AND 31. The concentration ranges of dAl and lpAl in the Kuroshio region (AND 06, 22, 31, and 34) were 1.37–12.4 and not detected (ND)–93.6 nmol/kg, respectively. These values are significantly higher than those observed in the Northern Pacific Ocean (Zheng et al. 2017). The vertical profiles of dAl in the ECS exhibited a scavenging profile, which are similar to those observed in the Indian Ocean (Vu and Sohrin 2013) and the Northern Pacific Ocean (Zheng et al. 2019). dAl did not show a strong positive correlation with other parameters for all data in this study (Table 1).

The sectional distribution of lpAl is generally similar to that of the other lpMs (Fig. 8). The correlation coefficients between lpAl and the other lpMs were higher than 0.90 for all data (Table 3). These results indicate that aluminosilicate particles are a major factor that dominates the distribution of lpMs. Concentration peaks for lpAl were observed at depths of 595 m (AND 06), 794 m (AND 22), 949 m (AND 31), and 991 m (AND 34) in the Kuroshio region. The vertical profiles of the lpAl/tdAl ratio are shown in Fig. 9(A). The statistical data of the lpAl/tdAl ratios are shown in Table 2. The lpAl/tdAl ratios for AND 06 were 0.11 ± 0.12 (ave \pm sd, $n = 10$) at a depth of ≤ 400 m and 0.76 ± 0.09 ($n = 4$) at > 400 m; those for AND 22 were 0.23 ± 0.27 ($n = 9$) at ≤ 400 m and 0.91 ± 0.05 ($n = 6$) at > 400 m; those for AND 26 were 0.57 ± 0.26 ($n = 8$) at ≤ 100 m; those for AND 31 were 0.08 ± 0.07 ($n = 8$) at ≤ 400 m and 0.85 ± 0.11 ($n = 5$) at > 400 m; and those for AND 34 were 0.13 ± 0.07 ($n = 9$) at ≤ 400 m and 0.82 ± 0.05 ($n = 8$) at a depth of > 400 m. These results indicate that lpAl was the dominant species of Al at a depth of > 400 m at any of the sampling stations.

4.3 Mn

The full depth vertical profiles of dMn and lpMn are shown in Figs. 5(B) and 7(B), respectively. The sectional distributions of dMn and lpMn are shown in Figs. 6(B) and 8(B), respectively. The concentration ranges of dMn and lpMn at AND 26, in the continental shelf region, were 2.06–2.92 and 1.28–49.3 nmol/kg, respectively. These concentrations of Mn at AND 26 were substantially higher than those in the Kuroshio region in a similar manner to Al. The concentration ranges of dMn and lpMn in the Kuroshio region (AND 06, 22, 31, and 34) were 0.30–7.48 and ND–11.9 nmol/kg, respectively. The vertical profiles of dMn exhibited a scavenging profile, which are similar to those observed in the North Pacific (Bruland et al 1994; Zheng et al. 2019) and

the Atlantic Ocean (Saager et al. 1997). However, the concentrations of dMn and lpMn increased sharply at the bottom layer at AND 22 and 31. The sources of dMn may be attributed to manganese reduction in sediments (Wang et al. 2016) and/or hydrothermal activity in the Okinawa Trough (Hsu et al. 2003A). Subsequently, dMn is oxidized to form Mn oxides in the water column, resulting in a unique distribution of lpMn. dMn did not show a strong correlation with other parameters for all data in this study (Table 1). In addition, lpMn did not show a strong correlation with the other lpMs in the Kuroshio region of the ECS (Table 3).

The vertical profiles of lpMn/tdMn are shown in Fig. 9(B). The statistical data of the lpMn/tdMn ratios are shown in Table 2. The lpMn/tdMn ratios for AND 06 were 0.19 ± 0.15 ($n = 10$) at a depth of ≤ 400 m and 0.57 ± 0.07 ($n = 4$) at > 400 m; those for AND 22 were 0.19 ± 0.19 ($n = 9$) at ≤ 400 m and 0.69 ± 0.12 ($n = 6$) at > 400 m; those for AND 26 were 0.50 ± 0.28 ($n = 8$) at ≤ 100 m; those for AND 31 were 0.13 ± 0.17 ($n = 8$) at ≤ 400 m and 0.58 ± 0.23 ($n = 5$) at > 400 m; and those for AND 34 were 0.20 ± 0.13 ($n = 9$) at ≤ 400 m and 0.51 ± 0.07 ($n = 8$) at > 400 m. Thus, the lpMn/tdMn ratios were lower than the lpAl/tdAl ratios.

4.4 Fe

The full depth vertical profiles of dFe and lpFe are shown in Figs. 5(C) and 7(C), respectively. The sectional distributions of dFe and lpFe are shown in Figs. 6(C) and 8(C), respectively. The concentration ranges of dFe and lpFe at AND 26, in the continental shelf region, were 0.30–1.26 and 0.76–7.60 nmol/kg, respectively. The concentration ranges of dFe and lpFe in the Kuroshio region (AND 06, 22, 31, and 34) were 0.26–1.46 and ND–67.7 nmol/kg, respectively. These concentrations are consistent with those at the shelf edge slope in the ECS (Sasayama et al. 2018). The vertical profiles of dFe exhibited a nutrient-like profile in a similar manner to those observed in the Gulf of Alaska (Martin et al. 1989) and the Northern Pacific Ocean (Zheng and Sohrin 2019). However, dFe was not depleted in surface water in this area. This may be because the flux of dFe to the surface water is higher than the uptake rate of dFe by phytoplankton. dFe showed a maximum around $\sigma_0 = 26.0$ – 27.5 . Such a maximum has been observed near continents in both the northwestern and northeastern North Pacific (Zheng and Sohrin 2019). dFe showed a moderate correlation with NO_3 and PO_4 for all data in this study (Table 1). A correlation plot of dFe with PO_4 is shown in Fig. 10(A). The regression lines between nutrient concentrations and dissolved metal concentrations are listed in Table S4 (online supplementary material). The regression lines for dFe in the ECS are as follows:

$$d\text{Fe} [\text{nmol/kg}] = (0.017 \pm 0.002) \text{NO}_3 [\mu\text{mol/kg}] + (0.596 \pm 0.051) \quad r^2 = 0.65, n = 44$$

$$d\text{Fe} [\text{nmol/kg}] = (0.191 \pm 0.028) \text{PO}_4 [\mu\text{mol/kg}] + (0.665 \pm 0.062) \quad r^2 = 0.57, n = 38$$

The relationship between dFe and NO₃ is similar to the results in the Gulf of Alaska (Martin et al. 1989):

$$d\text{Fe} [\text{nmol/kg}] = 0.0137 \text{NO}_3 [\mu\text{mol/kg}] - 0.0619 \quad r^2 = 0.85, n = 14$$

The distribution of lpFe was close to that of lpAl (Table 3). The concentration peaks for lpFe were observed at depths of 595 m (AND 06), 794 m (AND 22), 949 m (AND 31), and 991 m (AND 34). The vertical profiles of lpFe/tdFe are shown in Fig. 9(C). The statistical data of the lpFe/tdFe ratios are shown in Table 2. The lpFe/tdFe ratios for AND 06 were 0.52 ± 0.27 ($n = 10$) at a depth of ≤ 400 m and 0.88 ± 0.01 ($n = 4$) at > 400 m; those for AND 22 were 0.68 ± 0.17 ($n = 9$) at ≤ 400 m and 0.95 ± 0.02 ($n = 6$) at > 400 m; that for AND 26 was 0.75 ± 0.19 ($n = 8$) at ≤ 100 m; those for AND 31 were 0.41 ± 0.28 ($n = 8$) at ≤ 400 m and 0.92 ± 0.04 ($n = 5$) at > 400 m; and those for AND 34 were 0.60 ± 0.06 ($n = 9$) at ≤ 400 m and 0.84 ± 0.05 ($n = 8$) at a depth of > 400 m. These results suggest that lpFe was the dominant species of Fe at a depth of > 400 m at any of the sampling stations in a similar manner to Al.

4.5 Co

The full depth vertical profiles of dCo and lpCo are shown in Figs. 5(D) and 7(D), respectively. The sectional distributions of dCo and lpCo are shown in Figs. 6(D) and 8(D), respectively. The concentration ranges of dCo and lpCo at AND 26, in the continental shelf region, were 30.2–106 and 24.3–731 pmol/kg, respectively. The concentration ranges of dCo and lpCo in the Kuroshio region (AND 06, 22, 31, and 34) were 1.24–56.5 and ND–23.1 pmol/kg, respectively. dCo exhibited maxima at the surface and mid-depth. The mid-depth peaks of dCo were observed at 695 (AND 06), 595 (AND 22), 498 (AND 31), and 596 m (AND 34), where dFe had peaks simultaneously. Below the mid-depth peaks, dCo decreased with depth. These results are consistent with the unique marine chemistry of Co, i.e., it is neither a typical nutrient-type nor a scavenged-type element. The distribution of dCo in the Sulu Sea and South China Sea is a scavenged-type with surface enrichment and decreases with depth (Norisuye et al. 2007). The distribution of dCo in the subtropical Atlantic was nutrient-like, with low levels in surface waters and the lowest concentrations observed where Chl. *a* was the highest (Bown et al. 2011). A similar distribution of surface depletion of dCo has been observed in the South Pacific (Ellwood 2008), in the eastern North Pacific (Martin et al. 1989), North Atlantic

(Martin et al. 1993), and Sargasso Sea (Saito and Moffett 2001). Biological uptake by cyanobacteria is the dominant removal mechanism for cobalt in the surface waters of the oligotrophic Sargasso Sea (Saito and Moffett 2001). At station AND 06, dCo showed the lowest concentration at which Chl. *a* had the maximum concentration. Thus, biological uptake in the euphotic layer and remineralization from biological particles at depth is a major process to determine the distribution of Co in the ECS. dCo showed a moderate correlation with dFe and weak correlations with NO₃ and PO₄ for all data in this study (Table 1). A correlation plot of dCo with PO₄ is shown in Fig. 10(B). The regression lines for dCo in the ECS are as follows:

$$\text{dCo [pmol/kg]} = (0.529 \pm 0.107) \text{NO}_3 [\mu\text{mol/kg}] + (19.4 \pm 2.8) \quad r^2 = 0.37, n = 44$$

$$\text{dCo [pmol/kg]} = (5.72 \pm 1.59) \text{PO}_4 [\mu\text{mol/kg}] + (21.7 \pm 3.6) \quad r^2 = 0.26, n=38$$

lpCo does not show a significant correlation with any other lpM in the Kuroshio region (Table 3). The vertical profiles of the lpCo/tdCo ratio are shown in Fig. 9(D). The statistical data of the lpCo/tdCo ratios are shown in Table 2. The lpCo/tdCo ratios for AND 06 were 0.33 ± 0.14 ($n = 10$) at a depth of ≤ 400 m and 0.15 ± 0.12 ($n = 4$) at > 400 m; those for AND 22 were 0.28 ± 0.36 ($n = 9$) at ≤ 400 m and 0.10 ± 0.03 ($n = 6$) at > 400 m; that for AND 26 was 0.43 ± 0.32 ($n = 8$) at ≤ 100 m; those for AND 31 were 0.02 ± 0.04 ($n = 8$) at a depth of ≤ 400 m and 0.29 ± 0.22 ($n = 5$) at > 400 m; and those for AND 34 were 0.14 ± 0.14 ($n = 9$) at ≤ 400 m and 0.22 ± 0.08 ($n = 8$). These results indicate that lpCo is a minor chemical species in tdCo.

4.6 Ni

The full-depth vertical profiles of dNi are shown in Fig. 5(E). The sectional distribution of dNi is shown in Fig. 6(E). The concentration range of dNi at AND 26, in the continental shelf region, was 3.42–4.82 nmol/kg. The concentration range of dNi in the Kuroshio region (AND 06, 22, 31, and 34) was 2.46–10.7 nmol/kg. dNi exhibited a nutrient-like profile. dNi showed a strong correlation with Si(OH)₄, NO₃, and PO₄ for all data in this study (Table 1). It is well known that there is a significant positive correlation between dNi and nutrients in the North Pacific (Bruland 1980; Ezoe 2004), in the South China Sea (Wen et al. 2006), and in the Tasman Sea (Ellwood 2008). A correlation plot of dNi with PO₄ is shown in Fig. 10(C). The regression lines for dNi in the ECS are as follows:

$$\text{dNi [nmol/kg]} = (0.053 \pm 0.002) \text{Si(OH)}_4 [\mu\text{mol/kg}] + (3.44 \pm 0.15) \quad r^2 = 0.97, n = 31$$

$$\text{dNi [nmol/kg]} = (0.188 \pm 0.006) \text{NO}_3 [\mu\text{mol/kg}] + (2.41 \pm 0.15) \quad r^2 = 0.96, n = 44$$

$$\text{dNi [nmol/kg]} = (2.39 \pm 0.096) \text{PO}_4 [\mu\text{mol/kg}] + (2.23 \pm 0.22) \quad r^2 = 0.95, n = 38$$

These relations are in good agreement with the results in the northern North Pacific shown

below (Ezoe et al. 2004):

$$\text{dNi [nmol/kg]} = 0.043 \text{ Si(OH)}_4 [\mu\text{mol/kg}] + 2.83 \quad r^2 = 0.96, n=159$$

$$\text{dNi [nmol/kg]} = 0.182 \text{ NO}_3 [\mu\text{mol/kg}] + 1.90 \quad r^2 = 0.92, n=151$$

$$\text{dNi [nmol/kg]} = 2.54 \text{ PO}_4 [\mu\text{mol/kg}] + 1.92 \quad r^2 = 0.92, n=171$$

lpNi was observed only in the bottom waters at AND 26 and 34.

4.7 Cu

The full-depth vertical profiles of dCu are shown in Fig. 5(F). The sectional distribution of dCu is shown in Fig. 6(F). The concentration range of dCu at AND 26 was 0.98–1.96 nmol/kg. The concentration range of dCu in the Kuroshio region (AND 06, 22, 31, and 34) was 0.29–3.42 nmol/kg. dCu showed high concentrations in surface water, a minimum around a depth of 150–200 m and increased with depth to the bottom. Similar distributions have been observed in the North Pacific (Boyle et al. 1977; Ezoe et al. 2004), the South China Sea (Wen et al. 2006), and the Sulu Sea (Norisuye et al. 2007). These vertical distributions of dCu have been explained by the hybrid effects of the biological uptake and remineralization and the particle scavenging in subsurface and deep layers. dCu showed the strongest correlation with Si(OH)₄ for all data in this study (Table 1). A correlation plot of dCu with PO₄ is shown in Fig. 10(D). The regression lines for dCu in the ECS are as follows:

$$\text{dCu [nmol/kg]} = (0.014 \pm 0.001) \text{ Si(OH)}_4 [\mu\text{mol/kg}] + (0.22 \pm 0.10) \quad r^2 = 0.85, n = 31$$

$$\text{dCu [nmol/kg]} = (0.038 \pm 0.004) \text{ NO}_3 [\mu\text{mol/kg}] + (0.32 \pm 0.10) \quad r^2 = 0.68, n = 44$$

$$\text{dCu [nmol/kg]} = (0.508 \pm 0.062) \text{ PO}_4 [\mu\text{mol/kg}] + (0.21 \pm 0.14) \quad r^2 = 0.65, n = 38$$

These results are consistent with previous studies showing a strong positive correlation between dCu and Si(OH)₄ in the ocean (Boyle et al. 1977; Bruland and Franks 1983; Jacquot and Moffett 2015; Roshan and Wu 2015). dCu exhibits a stronger correlation with Si(OH)₄ than with NO₃ and PO₄ (Jacquot and Moffett 2015).

lpCu was observed at AND 26 (0.28–1.06 nmol/kg) and in some samples in the upper water column at other stations.

4.8 Zn

The full-depth vertical profiles of dZn are shown in Fig. 5(G). The sectional distribution of dZn is shown in Fig. 6(G). The concentration range of dZn at AND 26 was 0.60–1.65 nmol/kg. The concentration range of dZn in the Kuroshio region (AND 06, 22, 31, and 34) was 0.42–11.3 nmol/kg. The vertical profiles of dZn showed a nutrient-type profile

in a similar manner to that observed in the North Pacific (Bruland et al. 1994; Ezoe et al. 2004), the Sulu Sea (Norisuye et al. 2007), and the Tasman Sea (Ellwood 2008). However, dZn was not depleted in surface water in the ECS, suggesting that the flux of dZn to the surface water is higher than the uptake rate of dZn by phytoplankton. dZn showed strong correlations with Si(OH)₄, NO₃, and PO₄ for all data in this study (Table 1). A correlation plot of dZn and PO₄ is shown in Fig. 10(E). The regression lines for dZn in the ECS are as follows:

$$\text{dZn [nmol/kg]} = (0.073 \pm 0.002) \text{ Si(OH)}_4 [\mu\text{mol/kg}] + (0.94 \pm 0.22) \quad r^2 = 0.97, n = 31$$

$$\text{dZn [nmol/kg]} = (0.236 \pm 0.011) \text{ NO}_3 [\mu\text{mol/kg}] + (0.32 \pm 0.29) \quad r^2 = 0.91, n = 44$$

$$\text{dZn [nmol/kg]} = (3.07 \pm 0.18) \text{ PO}_4 [\mu\text{mol/kg}] - (0.08 \pm 0.40) \quad r^2 = 0.89, n = 38$$

dZn exhibited a stronger correlation with Si(OH)₄ than with NO₃ and PO₄. A similar trend was observed in seawater samples collected from the North Pacific Ocean (Ezoe et al. 2004):

$$\text{dZn [nmol/kg]} = (0.054 \pm 0.001) \text{ Si(OH)}_4 [\mu\text{mol/kg}] + (1.73 \pm 0.13) \quad r^2 = 0.93, n = 157$$

$$\text{dZn [nmol/kg]} = (0.214 \pm 0.009) \text{ NO}_3 [\mu\text{mol/kg}] + (0.95 \pm 0.28) \quad r^2 = 0.79, n = 148$$

$$\text{dZn [nmol/kg]} = (2.966 \pm 0.111) \text{ PO}_4 [\mu\text{mol/kg}] + (1.01 \pm 0.23) \quad r^2 = 0.81, n = 169$$

lpZn was detected in bottom water at AND 26 and in some surface waters at AND 22 and 31.

4.9 Cd

The full depth vertical profiles of dCd are shown in Fig. 5(H). The sectional distribution of dCd is shown in Fig. 6(H). The concentration range of dCd at AND 26 was 0.03–0.12 nmol/kg. The concentration range of dCd in the Kuroshio region (AND 06, 22, 31, and 34) was ND–1.55 nmol/kg. The vertical profiles of dCd in the ECS showed a nutrient-type profile. Similar distributions have been observed in the North Pacific (Bruland 1980; Bruland et al. 1994; Ezoe et al. 2004), the Atlantic Ocean (Saager et al. 1997), the South China Sea (Wen et al. 2006), the Sulu Sea (Norisuye et al. 2007), and Tasman Sea (Ellwood 2008). The dCd concentrations in deep water in this study were significantly higher than typical concentrations in deep water in the North Pacific. This may be attributed to the luxury uptake of dCd in surface water and subsequent remineralization in deep water on the continental slope. dCd showed strong correlations with Si(OH)₄, NO₃, and PO₄ for all data in this study (Table 1). A correlation plot of dCd and PO₄ is shown in Fig. 10(F). The regression lines for dCd in the ECS are as follows:

$$\text{dCd [nmol/kg]} = (0.010 \pm 0.000) \text{ Si(OH)}_4 [\mu\text{mol/kg}] + (0.118 \pm 0.032) \quad r^2 = 0.97, n = 31$$

$$\text{dCd [nmol/kg]} = (0.035 \pm 0.001) \text{ NO}_3 [\mu\text{mol/kg}] - (0.062 \pm 0.031) \quad r^2 = 0.95, n = 44$$

$$dCd \text{ [nmol/kg]} = (0.444 \pm 0.019) PO_4 \text{ [\mu mol/kg]} - (0.093 \pm 0.043) \quad r^2 = 0.94, n = 38$$

lpCd was detected in a few samples in the upper water column at AND 6, 22, and 31. In contrast with other metals, lpCd was not detected at 26.

4.10 Pb

The full depth vertical profiles of dPb and lpPb are shown in Figs. 5(I) and 7(E), respectively. The sectional distributions of dPb and lpPb are shown in Figs 6(I) and 8(E), respectively. The concentration ranges of dPb and lpPb at AND 26, in the continental shelf region, were 68.0–108 and ND–270 pmol/kg, respectively. The concentration ranges of dPb and lpPb in the Kuroshio region (AND 06, 22, 31, and 34) were 15.8–83.0, and ND–32.4 pmol/kg, respectively. The vertical profiles of dPb showed a scavenging profile. A subsurface maximum occurred around $\sigma_0 = 24.0$ – 26.0 . The concentration peaks of dPb were observed at 298 m at AND 06, 247 m at AND 22, 198 m at AND 31, and 397 m at AND 34. Such subsurface maxima are similar to those observed in the North Pacific (Zheng et al. 2019).

The vertical profiles of lpPb/tdPb are shown in Fig. 9(E). The statistical data of the lpPb/tdPb ratios are shown in Table 2. The lpPb/tdPb ratios for AND 06 were 0.04 ± 0.00 ($n = 10$) at a depth of ≤ 400 m and 0.12 ± 0.06 ($n = 4$) at > 400 m; those for AND 22 were 0.09 ± 0.13 ($n = 9$) at ≤ 400 m and 0.26 ± 0.22 ($n = 6$) at > 400 m; those for AND 26 were 0.29 ± 0.29 ($n = 8$) at ≤ 100 m; those for AND 31 were 0.03 ± 0.06 ($n = 8$) at a depth of ≤ 400 m and 0.32 ± 0.16 ($n = 5$) at > 400 m; and those for AND 34 were 0.06 ± 0.04 ($n = 9$) at ≤ 400 m and 0.12 ± 0.04 ($n = 8$) at > 400 m. Thus, similar to lpCo, lpPb is a minor fraction of tdPb. Nonetheless, the sectional distribution of lpPb basically resembles that of lpAl, lpFe and lpCo (Fig. 8). However, lpPb did not show a significant correlation with any other lpM in the Kuroshio region (Table 3).

5 Discussions

5. 1. Labile particulate metals

There are many reports on the distribution of dissolved trace metals in the ocean, but few reports on the distribution of labile particulate metals. The concentrations of lpMs are operationally defined as the difference between tdMs and dMs. The lp species include (1) metal oxides, hydroxides, sulfides, and carbonates; (2) metal ions adsorbed on mineral surfaces; and (3) metal ions complexed with organic matter in suspended particles (Ezoe

et al. 2004). Zheng et al. (2019) found that Al is also released from aluminosilicate minerals after year-long storage, and presumed that lpMs represent a major portion of total particulate metals in the open ocean.

A strong linear relationship between lpFe and lpAl in the ECS was observed in the Kuroshio region of the ECS (Fig. 11) as follows:

$$\text{lpFe [nmol/kg]} = (0.687 \pm 0.016) \text{lpAl [nmol/kg]} + (0.05 \pm 0.44) \quad r^2 = 0.98, n = 41$$

Such a strong correlation between lpFe and lpAl has been reported in the North Pacific Ocean (Zheng and Sohrin 2019), where the slope is 0.544 ± 0.005 and the intercept is 0.11 ± 0.04 . Thus, the slope was significantly higher in the ECS. In general, a high positive correlation between the two components suggests that these two components are of the same origin. Atmospheric input of terrestrial materials is considered to be one of the origins of these lpM into the ECS. The average lpFe/lpAl ratio in the ECS was 0.66 ± 0.22 ($n = 41$). This average was of the same order of magnitude as the Fe/Al ratios in the crust (0.33) (Taylor 1964), aerosol over the ECS (0.32) (Hsu et al. 2010), and aerosol over the North Pacific (0.53) (Buck et al. 2006). Zhang et al. (1998) reported that the aerosol Fe/Al ratio (0.69) during an Asian dust storm was higher than the Fe/Al ratio (0.34) during non Asian dust storm. This result suggests that Asian dust storms may affect the lpFe/lpAl ratio. Wang et al. (2017) reported that Chl. *a* concentrations are highly correlated with dry deposition flux ratios of soluble Fe/Cu in ECS. This implies that phytoplankton uptakes Fe effectively. Thus, we propose that phytoplankton uptake may be another mechanism to increase the lpFe/lpAl ratio.

The lpM/tdM ratios and vertical profiles of lpM/tdM in the ECS are shown in Table 2 and Fig. 9, respectively. The lpAl/tdAl ratio is 0.57 ± 0.32 (ave \pm sd, $n = 49$), the lpMn/tdMn ratio is 0.41 ± 0.23 ($n = 56$), the lpFe/tdFe ratio is 0.74 ± 0.18 ($n = 63$), the lpCo/tdCo ratio is 0.30 ± 0.23 ($n = 47$), and the lpPb/tdPb ratio is 0.15 ± 0.17 ($n = 58$) at full depth. The lpFe/tdFe ratio below 400 m depth (0.89 ± 0.06) is almost the same as the lpAl/tdAl ratio (0.84 ± 0.09). However, the lpFe/tdFe ratio from the surface to 400 m (0.65 ± 0.16) is significantly higher than the other lpMs/tdMs ratios. Al and Fe form a trivalent cation in seawater, which has a high hydrolysis constant, resulting in effective adsorption onto particles and a resulting higher lpM/tdM ratio. In addition, Hsu et al. (2010) reported the solubility of trace metals in atmospheric aerosols over the ECS. The solubility was 5.1 ± 2.8 % (ave \pm sd) for Al, 7.7 ± 4.5 % for Fe, 49 ± 12 % for Mn, 36 ± 12 % for Co, and 45 ± 16 % for Pb (Hsu et al. 2010). However, these factors cannot explain why the lpFe/tdFe ratio was higher than that of the other elements at a depth of < 400 m. A main factor controlling the lpFe/tdFe ratio is phytoplankton uptake. Among the five metals, Co has the most extensive effects of biological activity on the distribution

next to Fe. The $lpCo/tdCo$ ratio was significantly high in some samples from shallow depths. This trend is also attributed to phytoplankton uptake.

5.2 Enrichment factor: elucidating sources of trace metals

The enrichment factor against crust (EF) has been used to elucidate the origin of metals in atmospheric aerosols (Rahn 1976). Similarly, EF was calculated for the purpose of estimating the origin of dMs in ECS. The EF of dM in seawater is defined in accordance with the EF in aerosol (Rahn 1976) as follows:

$$EF(dM) = (dM/dAl)_{\text{seawater}} / (M/Al)_{\text{upper crust}}$$

The $(M/Al)_{\text{upper crust}}$ is calculated in moles using concentrations published in a review (Rudnick and Gao 2005): 4.7×10^{-3} for Mn, 2.3×10^{-1} for Fe, 9.7×10^{-5} for Co, 2.7×10^{-4} for Ni, 1.5×10^{-4} for Cu, 3.4×10^{-4} for Zn, 2.7×10^{-7} for Cd, and 2.7×10^{-5} for Pb. The average values of $EF(dM)$ in the ECS and North Pacific are summarized in Table 4. The vertical profiles of $EF(dM)$ for dFe, dMn, dCo, and dPb are shown in Fig. 12. $EF(dM)$ in the ECS is generally lower than that in the North Pacific by one or two orders of magnitude. In the ECS, $EF(dM)$ in shallow water is lower than that in deep water except for $EF(dPb)$. This may be attributed to the uptake of dM from shallow water by phytoplankton. Only $EF(dFe)$ in the ECS is close to unity, suggesting that terrigenous sources are dominant for Fe.

Guo et al. (2014) reported the EF of aerosols over Huaniao Island in the ECS. The averages are 2.8 for Mn, 1.2 for Fe, 1.4 for Co, 14 for Ni, 138 for Cu, 106 for Zn, 581 for Cd, and 155 for Pb. They suggested that Cu, Zn, Cd, and Pb are primarily of anthropogenic origin. $EF(dPb)$ in the ECS is of the same order of magnitude as the $EF(Pb)$ in the ECS atmospheric aerosol. These results suggest that dPb is derived from anthropogenic aerosols. $EF(dMn)$, $EF(dCo)$, $EF(dNi)$, $EF(dCu)$, $EF(dZn)$, and $EF(dCd)$ in the ECS were substantially higher than the $EF(Mn)$, $EF(Co)$, $EF(Ni)$, $EF(Cu)$, $EF(Zn)$, and $EF(Cd)$ in the ECS atmospheric aerosol, respectively. This cannot be explained only by the difference in solubility from aerosol among Al and other metals because it is less than a factor of 10 (Hsu et al. 2010). There are three possible mechanisms for this. The first is the reduction of manganese in the shelf and slope sediments (Wang et al. 2016). The second is the contribution of Pacific seawater with high $EF(dMs)$. The third is riverine input from anthropogenic sources. At present, we cannot estimate the relative importance of these mechanisms.

The concentrations of dMs and lpMs at AND 26 are summarized in Table 5 in comparison with those observed in the offshore area of the Yangtze River (Su et al. 2017)

and on the continental shelf of the Bering Sea (Cid et al. 2011). The concentrations of dCo, dCu, and dZn are high in the offshore area of the Yangtze River, indicating anthropogenic input. It is possible that anthropogenic input influences the metal concentrations in the CDW at AND 26. On the other hand, manganese reduction occurs in the continental shelf sediments of the Bering Sea, affecting the metal concentrations in seawater. The concentrations of dMs and lpMs at AND 26 are generally in their ranges on the Bering Sea shelf. Thus, it is also possible that manganese reduction has a significant influence on the metal concentrations in CDW at AND 26.

In addition, the enrichment factor of labile particulate metals, $EF(lpMs)$, was investigated. $EF(lpMn)$ was 3.5–99, with an average of 33 ($n = 67$). $EF(lpFe)$ was 0.3–9.1, with an average of 3.0 ($n = 67$). $EF(lpCo)$ was 0.4–282, with an average of 41 ($n = 67$). $EF(lpPb)$ was 3.2–659 with an average of 126 ($n = 67$). Again, the $EF(lpFe)$ is close to unity, and the $EF(lpPb)$ is close to the EF in aerosol. However, $EF(lpMs)$ are generally higher than the EF in aerosol, suggesting the effects of additional sources, such as authigenic Mn and Fe oxyhydroxides adsorption and biological uptake. Moffett and Ho (1996) have reported that Co uptake onto suspended particles in Waquoit Bay was dominated by microbial oxidation similarly with Mn. In the Sargasso Sea, by contrast, Mn and Co uptake onto suspended particles were completely decoupled. It was proposed that Co uptake is due primarily to uptake by phytoplankton. At depths of 75–100 m at AND 26, substantially high concentrations were observed for lpAl, lpMn, lpCo, and lpPb, where $EF(lpMn)$ was 3.7, $EF(lpFe)$ was 0.8–2.0, $EF(lpCo)$ was 2.6, and $EF(lpPb)$ was 3.3–3.9. These results suggest that the bottom maximum of lpMn, lpCo, and lpPb is largely attributed to the terrigenous source.

5.3 dM/P ratio: interplay between trace metals and biological activity

For marine organisms to grow and proliferate, as well as nitrogen and phosphorus, various trace metals, such as Mn, Fe, Co, Ni, Cu, Zn, and Cd are required. Macronutrients, such as carbon, nitrogen, and phosphorus are taken up by phytoplankton at a constant ratio. The average molar ratio of carbon to the two principal nutrient elements in organic matter, nitrogen, and phosphorus is approximately 106:16:1, and the N:P ratio in seawater also follows this (Redfield et al., 1963). Because a number of dMs are essential for phytoplankton, the Redfield ratio might be extended and include trace metals as “an extended Redfield ratio.” Vu and Sohrin (2013) investigated the validity of the extended Redfield ratio using global dM stoichiometry data. The dM/P ratios in the ECS are shown in Fig. 13: (A) shallow water < 200 m and (B) deep water > 500 m. All dM/P ratios at

depths below 500 m in the ECS are similar to those of the North Pacific Deep Water (NPDW; 170.00W, 10.00N).

Fig. 13 (A) also shows the M/P ratio that has been observed in natural phytoplankton (Ho et al. 2007, Ho et al. 2009). The dM/P ratio at a depth shallower than 200 m in the ECS exhibited higher values than those observed in the NPDW, excluding Cd. The Mn/P, Co/P, Cu/P, Zn/P, and Cd/P ratios were within the same order of magnitude for both phytoplankton and shallow water, whereas the Al/P and Fe/P ratios in phytoplankton were 27 and 213 times higher than those in seawater shallower than 200 m, respectively. Generally, upwelling deep water is the main source of nutrients for phytoplankton in the euphotic zone in the open ocean. Our results suggest that sufficient amounts of Mn, Co, Cu, Zn, and Cd are supplied in the ECS, as well as nutrients such as nitrate and phosphate. However, Fe could be a limiting factor for the growth of phytoplankton, although dFe was not exhausted in surface water in this study. When the biomass of phytoplankton increases, it is probable that dFe will become deficient earlier than any other essential nutrient and trace metal to limit the primary production. **Su et al. (2018) has proposed the possible Fe limitation in ECS.** Several research groups have studied the impact of Fe supply by Asian dust storms on the biogeochemistry of the ECS (Yuan and Zhang 2006; Hsu et al. 2009). These results are consistent with our results.

Fig. 13 (B) shows the M/P ratio in deep water in this area is generally close to that in NPDW. However, the Mn/P, Co/P, and Pb/P ratios are higher than those in NPDW, suggesting the occurrence of local sources for these metals.

6 Conclusions

This study has revealed the sectional distributions of Al, Mn, Fe, Co, Ni, Cu, Zn, Cd, and Pb in the fractions of td, d, and lp in the ECS. High concentrations of dAl, dMn, dCo, dCu, dPb, lpAl, lpMn, lpFe, lpCo, and lpPb were observed at the sampling point in the continental shelf region. At all the ESC stations, except in the continental shelf region, dAl showed a scavenging profile. dFe, dNi, dCu, dZn, and dCd showed a nutrient-like profile. dMn showed maxima in deep water and bottom water, suggesting supply from anoxic sediments and/or hydrothermal activity. dFe and dCo showed a maximum around $\sigma_0 = 26.0\text{--}27.5$, indicating intensive remineralization from settling particles. dPb showed a maximum around $\sigma_0 = 24.0\text{--}26.0$, which was consistent with that observed in the North Pacific. lpFe and lpAl showed almost the same vertical distribution, and a strong positive correlation was observed between these two components. From the results of lpM/tdM

ratios, it was found that lpFe and lpAl were the dominant species of tdFe and tdAl, respectively, below 400 m. The *EF* results suggested that only dFe is dominated by terrigenous supply as well as dAl, while the other dMs have significant additional sources. The dM/P results suggested that dFe could be a limiting factor for the growth of phytoplankton in the ECS, although dFe was not exhausted in surface water.

Acknowledgements

We are grateful to the Captain and the crew of R/V Hakuho-Maru (JAMSTEC) for their help during the KH-15-3 cruise. We also thank onboard scientists, technicians, and students for assistance with sampling and analysis of routine data. This research was supported by the Japan Society for the Promotion of Science (JSPS) KAKENHI grants (15H01727 and 19H01148) and the Collaborative Research Program of Institute for Chemical Research, Kyoto University grants (2016-43 and 2017-43). We would like to thank Editage (www.editage.com) for English language editing.

Electronic supplementary material

Figure captions

Fig. 1 Locations of sampling stations during the KH-15-3 cruise of R/V Hakuho Maru from October 14 to November 2 2015.

Fig. 2 Potential temperature (θ) and salinity diagram.

Fig. 3 Full depth vertical distributions of potential density anomaly, potential temperature, salinity, dissolved oxygen, nitrate, nitrite, phosphate, and silicic acid.

Fig. 4 Sectional distributions of potential temperature, salinity, dissolved oxygen, nitrate, nitrite, phosphate, and silicic acid from the surface to a depth of 1500 m between AND 26 and AND 34.

Fig. 5 Full depth vertical distributions of dAl, dMn, dFe, dCo, dNi, dCu, dZn, dCd, and dPb. Red circles, AND 6; brown triangles, AND 22; purple diamonds, AND 26; green squares, AND 31; grey reverse triangles, AND 34.

Fig. 6 Sectional distributions of dAl, dMn, dFe, dCo, dNi, dCu, dZn, dCd, and dPb from the surface to a depth of 1500 m between AND 26 and AND 34.

Fig. 7 Full depth vertical distributions of lpAl, lpMn, lpFe, lpCo, and lpPb. Red circles, AND 6; brown triangles, AND 22; purple diamonds, AND 26; green squares, AND 31; grey reverse triangles, AND 34.

Fig. 8 Sectional distributions of lpAl, lpMn, lpFe, lpCo, and lpPb from the surface to a depth of 1500 m between AND 26 and AND 34.

Fig. 9 Full depth vertical distributions of lpAl/tdAl, lpMn/tdMn, lpFe/tdFe, lpCo/tdCo, and lpPb/tdPb. Red circles, AND 6; brown triangles, AND 22; purple diamonds, AND 26; green squares, AND 31; grey reverse triangles, AND 34.

Fig.10 The relationship between dissolved metals and phosphate. (A) dFe, (B) dCo, (C) dNi, (D) dCu, (E) dZn, (F) dCd. Red circles, AND 6; brown triangles, AND 22; purple diamonds, AND 26; green squares, AND 31; grey reverse triangles, AND 34.

Fig. 11 The relationship between lpAl and lpFe in the Kuroshio region of the ECS. Red circles, AND 6; brown triangles, AND 22; green squares, AND 31; grey reverse triangles, AND 34.

Fig. 12 Full depth vertical distributions of $EF(dMn)$, $EF(dFe)$, $EF(dCo)$, and $EF(dPb)$. Red circles, AND 6; brown triangles, AND 22; purple diamonds, AND 26; green squares, AND 31; grey reverse triangles, AND 34.

Fig. 13 Bar plots of dM/P ratios at stations in this study. (1) shallow water < 200 m and (2) deep water > 500 m. (1) Circle plots of the M/P ratio that has been observed in natural phytoplankton (Ho et al. 2007, Ho et al. 2009).

Table titles

Table 1 Correlation matrix(r) of nutrients and dissolved trace metals for the pooled data collected in the East China Sea.

Table 2 The lpM/tdM ratios for Al, Mn, Fe, Co, and Pb in the East China Sea and the North Pacific.

Table 3 Correlation coefficients (r) among libile particulate species.

Table 4 The enrichment factor of dMs in the East China Sea and the North Pacific

Table 5 Concentrations of dMs and lpMs

References

- Abe K (2002) Relationship between Cd and PO₄ in the Subtropical Sea near the Ryukyu Islands. *J Oceanogr* 58, 577–588.
- Beardsley RC, Limeburner R, Yu H, Cannon GA (1985) Discharge of the Changjiang (Yangtze River) into the East China Sea, *Cont Shelf Res* 4, 57-76.
- Boye M, Wake BD, Lopez Garcia P, Bown J, Baker AR, Achterberg EP (2012) Distributions of dissolved trace metals (Cd, Cu, Mn, Pb, Ag) in the southeastern atlantic and the southern ocean. *Biogeosciences* 9, 3231–3246. doi:10.5194/bg-9-3231-2012.
- Boyle EA (1988) Cadmium: chemical tracer of deep water paleoceanography. *Paleoceanography* 3, 471–489.
- Boyle EA, Edmond JM (1975) Copper in surface waters south of New Zealand. *Nature* 253, 107–109.
- Boyle EA, Sclater FR, Edmond JM (1977) The distribution of dissolved copper in the Pacific. *Earth Planet Sci Lett* 37(1), 38-54. doi:10.1016/0012-821X(77)90144-3.
- Bown J, Boye M, Baker A, Duvieilbourg E, Lacan F, Moigne FL, Planchon F, Speich S, Nelson DM (2011) The biogeochemical cycle of dissolved cobalt in the Atlantic and the Southern Ocean south off the coast of South Africa, *Mar Chem* 126, 193-206. doi:10.1016/j.marchem.2011.03.008.
- Brown MT, Lippiatt SM, Bruland KW (2010) Dissolved aluminum, particulate aluminum, and silicic acid in northern Gulf of Alaska coastal waters: glacial/riverine inputs and extreme reactivity. *Mar Chem* 122, 160–175. doi:10.1016/j.marchem.2010.04.002.
- Bruland KW (1980) Oceanographic distributions of cadmium, zinc, nickel, and copper in the north Pacific. *Earth Planet Sci Lett* 47, 176–198.
- Bruland KW, Franks RP (1983) Mn, Ni, Cu, Zn and Cd in the western North Atlantic. In: Wong, C.S., Boyle E, Bruland KW, Burton JD, Goldberg ED (Eds.), *Trace Metals in Seawater*. Plenum, New York, pp. 395–415.
- Bruland KW, Orians, KJ, Cowen, JP (1994) Reactive trace metals in the stratified central North Pacific, *Geochim. Cosmochim. Acta*, 58, 3171-3182.
- Buck CS, Landing WM, Resing JA, Lebon GT(2006) Aerosol iron and aluminum solubility in the northwest Pacific Ocean: Results from the 2002 IOC cruise. *Geochem. Geophys. Geosyst.* 7, Q04M07. doi.org/10.1029/2005GC000977.
- Chang PH, Isobe A (2003) A numerical study of the Changjiang diluted water in the Yellow and East China Seas, *J Geophys Res* 108(C9), 3299.

- doi:10.1029/2002JC001749, 2003.
- Chen C, Beardsley RC, Limeburner R, Kim K (1994) Comparison of winter and summer hydrographic observations in the Yellow and East China Sea and adjacent Kuroshio during 1986, *Cont Shelf Res* 14, 909-959.
- Chen CA (1996) The Kuroshio intermediate water is the major source of nutrients on the East China Sea continental shelf, *Oceanologica Acta* 19(5), 523-527.
- Cid AP, Urushihara S, Minami T, Norisuye K, Sohrin Y (2011) Stoichiometry among bioactive trace metals in seawater on the Bering Sea shelf, *J Ocenogr* 67(6):747-764. doi: 10.1007/s10872-011-0070-z.
- Cid AP, Nakatsuka S, Sohrin Y (2012) Stoichiometry among bioactive trace metals in the Chukchi and Beaufort Seas. *Journal of Oceanography*, 68(6): 985-1001
- Dagg M, Benner R, Lohrenz S, Lawrence D (2004) Transformation of dissolved and particulate materials on continental shelves influenced by large river: Plume processes, *Cont Shelf Res* 24, 833-853. doi:10.1016/j.csr.2004.02.003.
- Danielson LG, Magnusson B, Westerlund S (1985) Cadmium, copper, iron, nickel and zinc in the north-east Atlantic Ocean. *Mar Chem* 17, 23–41.
- Ellwood MJ (2008) Wintertime trace metal (Zn, Cu, Ni, Cd, Pb and Co) and nutrient distributions in the Subantarctic Zone between 40–52°S; 155–160°E, *Mar Chem* 112, 107-117. Doi:10.1016/j.marchem.2008.07.008
- Ellwood MJ, Hunter KA (2000) The incorporation of zinc and iron into the frustule of the marine diatom *Thalassiosira pseudonana*. *Limnology and Oceanography*, 45(7): 1517-1524.
- Ezoe M, Ishita T, Kinugasa M, Lai X, Norisuye K, Sohrin Y (2004) Distributions of dissolved and acid-dissolved bioactive trace metals in the North Pacific. *Geochem J* 38(6), 535-550.
- Fitzwater SE (2000) Trace metal concentration in Ross Sea and their relationship with nutrients and phytoplankton growth. *Deep Sea Res II* 47, 3159–3179.
- Fitzwater SE, Johnson KS, Gordon RM, Coale KH, Smith WO (2000) Trace metal concentrations in the Ross Sea and their relationship with nutrients and phytoplankton growth. *Deep Sea Res Part II — Topical Studies in Oceanography* 47 (15–16), 3159–3179.
- Gehlen M, Beck L, Calas G, Flank AM, Van Bennekom AJ, Van Beusekom JEE (2002) Unraveling the atomic structure of biogenic silica: evidence of the structural association of Al and Si in diatom frustules. *Geochim Cosmochim Acta* 66 (9), 1601–1609.
- Gledhill M, van den Berg CMG (1994) Determination of complexation of iron(III) with

- natural organic complexing ligands in seawater using cathodic stripping voltammetry. *Mar Chem* 47 (1), 41–54. doi:10.1016/0304-4203(94)90012-4
- Guo L, Chen, Y, Wang F, Meng X, Xu Z, Zhuang G (2014) Effects of Asian dust on the atmosphere input of trace elements to the East China Sea, *Mar Chem* 163 19-27, doi.org/10.1016/j.marchem.2014.04.003
- Hall IR, Measures CI (1998) The distribution of Al in the IOC stations of the North Atlantic and Norwegian Sea between 52° and 65° North, *Mar Chem* 61(1-2), 69–85. doi:10.1016/S0304-4203(98)00008-5
- Heller MI, Croot PL (2015) Copper speciation and distribution in the Atlantic sector of the southern ocean. *Mar Chem*, 173(20), 253–268. doi:10.1016/j.marchem.2014.09.017
- Hernandez-Candelario IDG, Lares ML, Camacho-Ibar VF, Linacre L, Gutierrez-Mejia E, Perez-Brunius P (2019) Dissolved cadmium and its relation to phosphate in the deep region of the Gulf of Mexico, *J Mar Systems* 193, 27-45.
- Ho TY (2013) Nickel limitation of nitrogen fixation in *Trichodesmium*. *Limnology and Oceanography*, 58(1): 112-120.
- Ho TY, Wen LS, You CF, Lee DC (2007) The trace-metal composition of size-fractionated plankton in the South China Sea: Biotic versus abiotic sources. *Limnol Ocenogr* 52(5), 1776-1788.
- Ho TY, You CF, Chou WC, Pai SC, Wen LS, Sheu DD (2009) Cadmium and phosphorus cycling in the water column of the South China Sea: The roles of biotic and abiotic particles. *Mar Chem* 115, 125-133. doi:10.1016/j.marchem.2009.07.005.
- Hsu SC, Lin FJ, Jeng WL, Chung YC, Shaw LM (2003A) Hydrothermal signatures in the southern Okinawa Trough detected by the sequential extraction of settling particles. *Marine Chemistry*, 84(1-2): 49-66.
- Hsu SC, Lin FJ, Jeng WL, Tang TY (2003B) Spatial distribution of cadmium over a cyclonic eddy in the southern East China Sea, *J Mar Systems*, 39(3-4), 153-166. doi:10.1016/S0924-7963(03)00028-9
- Hsu SC, Liu SC, Arimoto R, Liu TH, Huang YT, Tsai F, Lin FJ, Kao SJ (2009) Dust deposition to the East China Sea and its biogeochemical implications, *J Geophys Res* 114, D15304, doi:10.1029/2008JD011223, 2009
- Hsu SC, Wong GTF, Gong GC, Shiah FK, Huang YT, Kao SJ, Tsai F, Lung SC, Lin FJ, Lin II, Hung CC, Tseng CM (2010) Source, solubility, and dry deposition of aerosol trace elements over the East China Sea. *Mar Chem* 120(1-4), 116-127. doi: 10.1016/j.marchem.2008.10.003.

- Hunter KA, Ho FWT (1991) Phosphorus-cadmium cycling in the northeast Tasman Sea, 35-40°S, *Mar Chem* 33(3), 279–298. doi:10.1016/0304-4203(91)90072-5.
- Hydes DJ (1983) Distribution of aluminum in waters of the North East Atlantic 25° N to 35° N. *Geochim Cosmochim Acta* 47, 967–983.
- Hydes DJ, de Lange GJ, de Baar HJW (1988) Dissolved aluminum in the Mediterranean. *Geochim Cosmochim Acta* 52, 2107–2114.
- Ibisanmi E, Sander SG, Boyd PW, Bowie AR, Hunter KA (2011) Vertical distributions of iron-(III) complexing ligands in the Southern Ocean. *Deep Sea Res II Top Stud Oceanogr* 58 (21), 2113–2125.
- Ichikawa H, Beardsley RC (2002) The Current System in the Yellow and East China Seas. *J. Oceanogr* 58, 77-92.
- Jacquot JE, Moffett JW (2015) Copper distribution and speciation across the International GEOTRACES Section GA03, *Deep-Sea Research II* 116, 187–207. doi.org/10.1016/j.dsr2.2014.11.013
- Janssen DJ, Cullen JT (2015) Decoupling of zinc and silicic acid in the subarctic northeast Pacific interior. *Marine Chemistry*, 177, Part 1: 124-133.
- Johns WE, Lee TN, Liu CT, Zhang D (1995) PCM-1 array monitors Kuroshio transport. *WOCE Notes* 7(3), 10-13.
- Kim T, Obata H, Nishioka J, Gamo T (2017) Distribution of Dissolved Zinc in the Western and Central Subarctic North Pacific. *Global Biogeochemical Cycles*, 31(9): 1454–1468.
- Klinkhammer GP, Bender ML (1980) The distribution of manganese in the Pacific Ocean. *Earth Planet Sci Lett* 46, 361–384.
- Kondo Y, Takeda S, Furuya K (2012) Distinct trends in dissolved Fe speciation between shallow and deep waters in the Pacific Ocean. *Mar Chem* 134(20), 18–28. doi:10.1016/j.marchem.2012.03.002.
- Kramer J, Laan P, Sarthou G, Timmermans KR, Baar HJW (2004) Distribution of dissolved aluminum in the high atmospheric input region of the subtropical waters of the North Atlantic Ocean. *Mar Chem* 88(3-4), 85–101. doi:10.1016/j.marchem.2004.03.009.
- Kraepiel AML, Chiffoleau JF, Martin JM, Morel FMM (1997) Geochemistry of trace metals in the Gironde estuary. *Geochim Cosmochim Acta* 61, 1421–1436.
- Landing WM, Bruland KW (1980) Manganese in the North Pacific. *Earth Planet Sci Lett* 49, 45–56.
- Landing WM, Bruland KW (1987) The contrasting biogeochemistry of iron and manganese in the Pacific Ocean, *Geochim Cosmochim Acta* 51, 29-43.

- Li Y, Yang R, Zhang A, Wang S (2014) The distribution of dissolved lead in the coastal waters of the East China Sea, *Mar Poll Bull* 85(2), 700-709. doi:10.1016/j.marpolbul. 2014.02.010.
- Lin FJ, Hsu SC, Jeng WL (2000) Lead in the southern East China Sea, *Mar Environ Res* 49(4), 329-342. doi:10.1016/S0141-1136(99)00076-8.
- Liu SM, Zhang J, Chen HT, Wu Y, Xiong H, Zhang ZF (2003) Nutrients in the Changjiang and its tributaries. *Biogeochemistry* 62, 1-18. doi:10.1023/A:1021162214304.
- Maldonado MT, Allen AE, Chong JS, Lin K, Leus D, Karpenko N, Harris SL (2006) Copper-dependent iron transport in coastal and oceanic diatoms. *Limnol Oceanogr* 51(4), 1729–1743.
- Martin JH, Fitzwater SE, Broenkow WW (1989) VERTEX: Phytoplankton/iron studies in the Gulf of Alaska, *Deep Sea Res* 36, 649-680.
- Martin JH, Fitzwater SE, Gordon RM, Hunter CN, Tanner SJ (1993) Iron, primary production and carbon-nitrogen flux studies during the JGOFS North Atlantic bloom experiment, *Deep Sea Research Part II: Topical Studies in Oceanography*, 40, 115-134.
- Martin JH, Gordon RM (1988) North Pacific iron distributions in relation to phytoplankton productivity, *Deep Sea Res* 35, 177-196.
- Martin JH, Gordon RM, Fitzwater SE (1990) Iron in Antarctic waters, *Nature* 345 (6271), 156-158.
- Martin JH, Gordon RM, Fitzwater SE, Broenkow, WW(1989) VERTEX: phytoplankton/iron studies in the Gulf of Alaska, *Deep-Sea Res* 36, 649-680.
- Measures CI, Edmond JM (1988) Aluminum as a tracer of the deep outflow from the Mediterranean, *J Geophys Res* 93, 591–595.
- Measures CI, Edmond JM, Jickells TD (1986) Aluminum in the northwest Atlantic, *Geochim Cosmochim Acta* 50, 1423–1429.
- Measures CI, Vink S. (1999) Seasonal variations in the distribution of Fe and Al in the surface waters of the Arabian Sea, *Deep-Sea Res II* 46, 1597–1622.
- Middag R, de Baar HJW, Laan P, Cai PH, Ooijen JC (2011) Dissolved manganese in the Atlantic sector of the Southern Ocean, *Deep-Sea Res II* 58, 2661-2677.
- Middag, R., de Baar, H.J.W., Bruland, K.W., van Heuven, S.M.A.C., (2020). The Distribution of Nickel in the West-Atlantic Ocean, Its Relationship With Phosphate and a Comparison to Cadmium and Zinc. *Frontiers in Marine Science*, 7: 105.
- Minami T, Konagaya W, Zheng L, Takano S, Sasaki M, Murata R, Nakaguchi Y, Sohrin

- Y, (2015) An off-line automated preconcentration system with ethylenediamine-triacetate chelating resin for the determination of trace metals in seawater by high-resolution inductively coupled plasma mass spectrometry, *Anal Chim Acta* 854, 183-190.
- Moffett JW, Ho J (1996) Oxidation of cobalt and manganese in seawater via a common microbially catalyzed pathway, *Geochim Cosmochim Acta*, 60, 3415-3424.
- Morel FMM, Milligan AJ, Saito MA (2003) Marine bioinorganic chemistry: The role of trace metals in the oceanic cycles of major nutrients, in: Elderfield H (Ed) *The Oceans and Marine Geochemistry. Treatise on Geochemistry*, Oxford Elsevier, pp. 113-143.
- Morel FMM, Price NM (2003) The biogeochemical cycles of trace metals in the oceans, *Science* 300, 944-947.
- Morris AW, Howland RJM, Bale AJ (1986) Dissolved aluminum in the Tamar estuary, southeast England, *Geochim Cosmochim Acta* 50, 189–197.
- Nitani H, (1972) Beginning of the Kuroshio. In: Stommel H, Yoshida K (Eds), *Kuroshio, Physical Aspects of the Japan Current*. University of Washington Press, Seattle, pp.129-163.
- Nolting RF, de Baar HJW (1994) Behaviour of nickel, copper, zinc and cadmium in the upper 300m of a transect in the Southern Ocean (57–62°S, 49°W), *Mar Chem* 45, 225–242. doi:10.1016/0304-4203(94)90006-X
- Norisuye K, Ezoe M, Nakatsuka S, Umetani S, Sohrin Y (2007) Distribution of bioactive trace metals (Fe, Co, Ni, Cu, Zn and Cd) in the Sulu Sea and its adjacent seas, *Deep-sea Res. Part II*, 54, 14-37
- Nozaki Y, Kasemsupaya V, Tsubota H (1989) Mean residence time of the shelf water in the East China and the Yellow Seas determined by $^{228}\text{Ra}/^{226}\text{Ra}$ measurements. *Geophys. Res. Lett.*, 16(11), 1297-1300. <https://doi.org/10.1029/GL016i011p01297>.
- Obata H, Nozaki Y, Alibo DS, Yamamoto Y (2004) Dissolved Al, In and Ce in the eastern Indian Ocean and the Southeast Asian Seas in comparison with the radionuclides ^{210}Pb and ^{210}Po , *Geochim Cosmochim Acta* 68, 1035–1048.
- Orians IJ, Bruland KW (1986) The biogeochemistry of aluminum in the Pacific Ocean, *Earth Planet Sci Lett* 78, 397–410.
- Öztürk M, Bizsel N, Steinnes E (2003) Iron speciation in eutrophic and oligotrophic Mediterranean coastal waters; impact of phytoplankton and protozoan blooms on iron distribution, *Mar Chem* 81 (1), 19–36. doi:10.1016/S0304-4203(02)00137-8

- Peers G, Price NM (2006) Copper-containing plastocyanin used for electron transport by an oceanic diatom, *Nature* 441 (7091), 341–344.
- Rahn KA (1976) Silicon and aluminum in atmospheric aerosols: Crust-air fractionation?, *Atmos Environ*, 10, 597-601.
- Redfield AC, Ketchum BH, Richards FA (1963) In *The Sea Vol.2* (ed Hill MN) 26-77 (Wiley).
- Ren JL, Zhang J, Li JB, Yu XY, Liu SM, Zhang ER (2006) Dissolved aluminum in the Yellow Sea and East China Sea – Al as a tracer of Changjiang (Yangtze River) discharge and Kuroshio incursion, *Estuarine Coastal and Shelf Sci* 68, 165-174. 10.1016/j.ecss.2006.02.004.
- Roshan S, Wu J (2015) The distribution of dissolved copper in the tropical-subtropical north Atlantic across the GEOTRACES GA03 transect, *Mar Chem* 176, 189-198. doi:10.1016/j.marchem.2015.09.006.
- Rue EL, Bruland KW (1995) Complexation of iron(III) by natural organic ligands in the Central North Pacific as determined by a new competitive ligand equilibration/adsorptive cathodic stripping voltammetric method, *Mar Chem* 50 (1), 117–138. doi:10.1016/0304-4203(95)00031-L
- Rudnick RL, Gao S (2005) Composition of the continental crust. In: *The Crust Treatise on Geochemistry* (ed Rudnick RL), Elsevier-Pergamon, pp.1–64,.
- Saager PM, de Baar HJW, de Jong JTM, Nolting RF, Schijf J (1997) Hydrography and local sources of dissolved trace metals Mn, Ni, Cu, and Cd in the northeast Atlantic Ocean, *Mar. Chem.*, 57, 195-216
- Saito MA, Moffet JW (2001) Complexation of cobalt by natural organic ligands in the Sargasso Sea as determined by a new high-sensitivity electrochemical cobalt speciation method suitable for open ocean work, *Mar Chem* 75, 49-68
- Saito MA, Moffet JW (2002) Temporal and spatial variability of cobalt in the Atlantic Ocean, *Geochim Cosmochim Acta* 66(11), 1943-1953.
- Saito MA, Moffet JW, Chisholm SW, Waterbury JB (2002) Cobalt limitation and uptake in *Prochlorococcus*, *Limnol Ocenogr* 47(6), 1629-1636.
- Saito MA, Moffett JW, DiTullio GR (2004) Cobalt and nickel in the Peru upwelling region: a major flux of labile cobalt utilized as a micronutrient. *Global Biogeochemical Cycles* 18 (4), GB4030.
- Sakamoto-Arnold CM, Hanson AK, Huizinga DL, Kester DR (1987) Spatial and temporal variability of cadmium in Gulf Stream warm core rings and associated waters, *J Mar Res* 45, 201–230.
- Sasayama R, Hioki N, Morita Y, Isoda Y, Imai K, Ooki A, Kuma K (2018) Upward

- transport of iron at the west shelf edge–slope of the Okinawa Trough in the East China Sea, *J Oceanogr* 1-13, doi:10.1007/s10872-018-0468-y.
- Schlitzer R (2015) Ocean Data View. <https://odv.awi.de>.
- SCOR Working Group (2007): GEOTRACES – An international study of the global marine biogeochemical cycles of trace elements and their isotopes. *Chemie der Erde-Geochemistry*, 67, 85-131. Doi:10.1016/j.chemer.2007.02.001.
- Sohrin Y, Urushihara S, Nakatsuka S, Kono T, Higo E, Minami T, Norisuye K, Umetani S (2008) Multielemental determination of GEOTRACES key trace metals in seawater by ICPMS after preconcentration using an ethylenediaminetriacetic acid chelating resin. *Anal Chem*, 80(16), 6267-6273. doi:10.1021/ac800500f.
- Statham PJ, Yeats PA, Landing WM (1998) Manganese in the eastern Atlantic Ocean: processes influencing deep and surface water distributions, *Mar Chem*(1-2) 61, 55-68. doi:10.1016/S0304-4203(98)00007-3.
- Su H, Yang R, Zhang A, Li Y (2015) Dissolved iron distribution and organic complexation in the coastal waters of the East China Sea, *Mar Chem* 173, 208-221. doi:10.1016/j.marchem.2015.03.007.
- Su H, Yang R, Zhang A, Li Y, Wang X (2018) Influence of humic substances on iron distribution in the East China Sea, *Chemosphere*, 204, 450-462. doi.org/10.1016/j.chemosphere.2018.04.018
- Su H, Yang R, Zhang A, Li Y, Qu S, Wang X (2017) Characteristics of trace metals and phosphorus in seawaters offshore the Yangtze River. *Marine Pollution Bulletin*, 124(2), 1020-1032.
- Sunda WG, Huntsman SA (1995) Cobalt and Zinc interreplacement in marine phytoplankton: Biological and geochemical implications, *Limnol Ocenogr* 40(8), 1404-1417.
- Sverdrup H U, Johnson M W, Fleming R H (1942) In: *The Oceans, Their Physics, Chemistry and General Biology*. Prentice Hall, Englewood Cliffs, NJ, p.719.
- Taylor SR (1964) Abundance of chemical elements in the continental crust: a new table, *Geochim Cosmochim Acta* 28, 1273-1285.
- Tebo B (1998) Mn(II) Oxidation in marine environments is likely bacterial: Comment on “Comment on ‘Oxidation of cobalt and manganese in seawater via a common microbially catalyzed pathway,’ by J. W. Moffett and J. Ho.” *Geochim Cosmochim Acta* 62, 357–358.
- Tebo B, Nealson K, Emerson S, Jacobs L (1984) Microbial mediation of Mn(II) and Co(II) precipitation at the O₂/H₂ interfaces in two anoxic fjords. *Limnol Oceanogr* 29, 1247–1258.

- Thompson CM, Ellwood MJ, Sander SG (2014) Dissolved copper speciation in the Tasman Sea, SW Pacific Ocean, *Mar Chem* 164, 84-94. doi:org/10.1016/j.marchem.2014.06.003.
- Vu HTD and Sohrin Y (2013) Diverse stoichiometry of dissolved trace metals in the Indian Ocean, *Scientific Report*, doi:10.1038/srep01745.
- Wang FJ, Chen Y, Guo ZG, Gao HW, Mackey KR, Yao XH, Zhuang GS, Paytan A (2017) Combined effects of iron and copper from atmospheric dry deposition on ocean productivity, *Geophys Res Letters*, 44, 2546–2555, doi:10.1002/2016GL072349.
- Wang RM, Archer C, Bowie AR, Vance D (2019) Zinc and nickel isotopes in seawater from the Indian Sector of the Southern Ocean: The impact of natural iron fertilization versus Southern Ocean hydrography and biogeochemistry. *Chemical Geology*, 511: 452-464.
- Wang ZW, Ren JL, Jiang S, Liu SM, Xuan JL, Zhang J (2016) Geochemical behavior of dissolved manganese in the East China Sea: Seasonal variation, estuarine removal, and regeneration under suboxic conditions, *Geochemistry, Geophysics, Geosystems*, 17(2), 282-299. doi:10.1002/2015GC006128.
- Wen LS, Jiann, KT, Santschi PH (2006) Physicochemical speciation of bioactive trace metals (Cd, Cu, Fe, Ni) in the oligotrophic South China Sea, *Mar. Chem.*, 101, 104-129. doi:10.1016/j.marchem.2006.01.005
- Windom HL, Smith RG, Maeda M (1985) The geochemistry of lead in rivers, estuaries and the continental shelf of the southeastern United States. *Mar Chem* 17(1), 43–56. doi:10.1016/0304-4203(85)90035-0
- Wu JF, Boyle EA (1997) Lead in the western North Atlantic Ocean: completed response to leaded gasoline phaseout, *Geochim Cosmochim Acta* 61 (15), 3279–3283.
- Wu J, Luther III GW (1994) Size-fractionated iron concentrations in the water column of the western North Atlantic Ocean, *Limnol Oceanogr* 39(5), 1119-1129.
- Wu J, Luther III GW (1995) Complexation of Fe (III) by natural organic ligands in the Northwest Atlantic Ocean by a competitive ligand equilibration method and a kinetic approach, *Mar Chem* 50 (1), 159–177. doi:10.1016/0304-4203(95)00033-N.
- Wu J, Roshan S, Chen G (2014) The distribution of dissolved manganese in the tropical–subtropical North Atlantic during US GEOTRACES 2010 and 2011 cruises, *Mar Chem* 166, 9-24. doi:10.1016/j.marchem.2014.08.007.
- Xie RC, Galer SJG, Abouchami W, Rijkenberg MJA, Jong JD, de Baar HJW, Andreae MO (2015) The cadmium-phosphate relationship in the western South Atlantic – The importance of mode and intermediate waters on the global systematics,

- Mar Chem 117, 110-123. doi:10.1016/j.marchem.2015.06.011.
- Yang R, Su H, Qu S, Wang X (2017) Capacity of humic substances to complex with iron at different salinities in the Yangtze River estuary and East China Sea, *Scientific Reports* 1. doi:10.1038/s41598-017-01533-6.
- Yuan W, Zhang J (2006) High correlations between Asian dust events and biological productivity in the western North Pacific, *Geophys Res Letters* 33, L07603, doi:10.1029/2005GL025174, 2006
- Zhang XY, Arimoto R, Zhu GH, Chen T, Zhang GY (1998) Concentration, size-distribution and deposition of mineral aerosol over Chinese desert regions, *Tellus*, 50B, 317-330.
- Zheng L, Minami T, Konagaya W, Chan C-Y, Tsujisaka M, Takano S, Norisuye K, Sohrin Y (2019) Distinct basin-scale-distributions of aluminum, manganese, cobalt, and lead in the North Pacific Ocean, *Geochim Cosmochim Acta* 254, 102-121. doi.org/10.1016/j.gca.2019.03.038
- Zheng L, Minami T, Takano S, Minami H, Sohrin Y (2017) Distribution and stoichiometry of Al, Mn, Fe, Co, Ni, Cu, Zn, Cd, and Pb in seawater around the Juan de Fuca Ridge, *J Oceanogr* 73, 669-685. doi:10.1007/s10872-017-0424-2.
- Zheng L and Sohrin Y (2019) Major lithogenic contributions to the distribution and budget of iron in the North Pacific Ocean, *Scientific Reports*, doi.org/10.1038/s41598-019-48035-1
- Zheng L, Minami T, Takano S, Ho T-Y, Sohrin Y, submitted. Sectional distribution patterns of Cd, Ni, Zn, and Cu in the North Pacific Ocean: Systematic importance of scavenging. *Global Biogeochemical Cycles*.

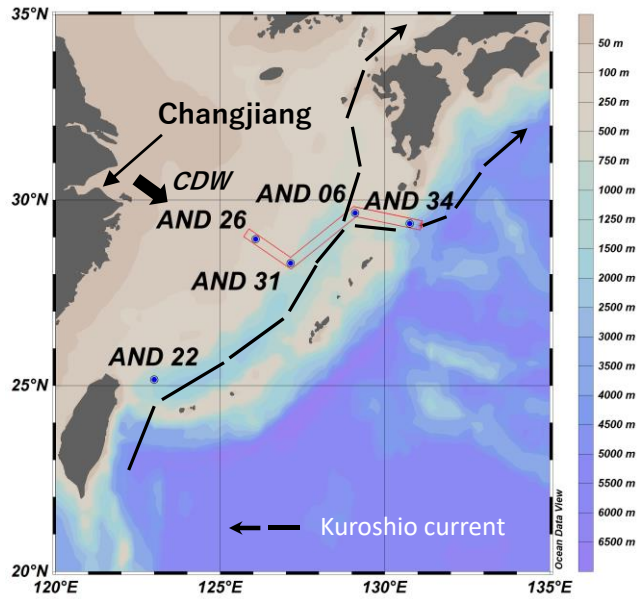


Fig.1 Nakaguchi et al

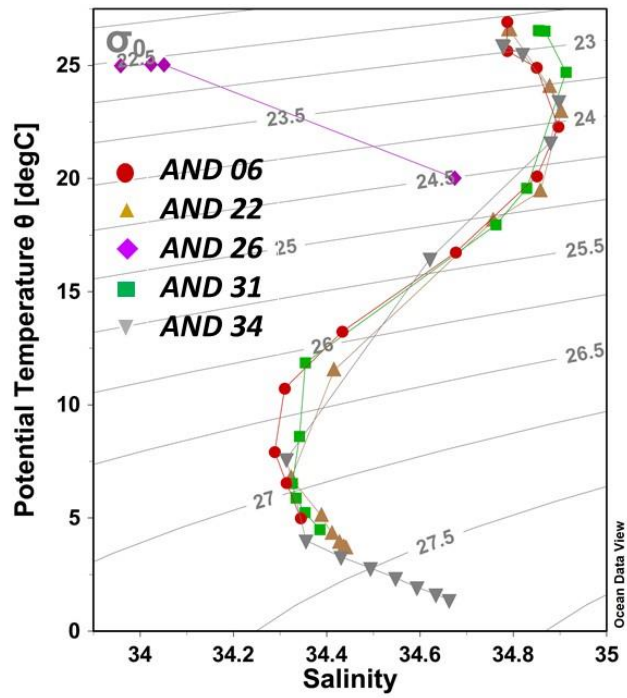


Fig.2 Nakaguchi et al

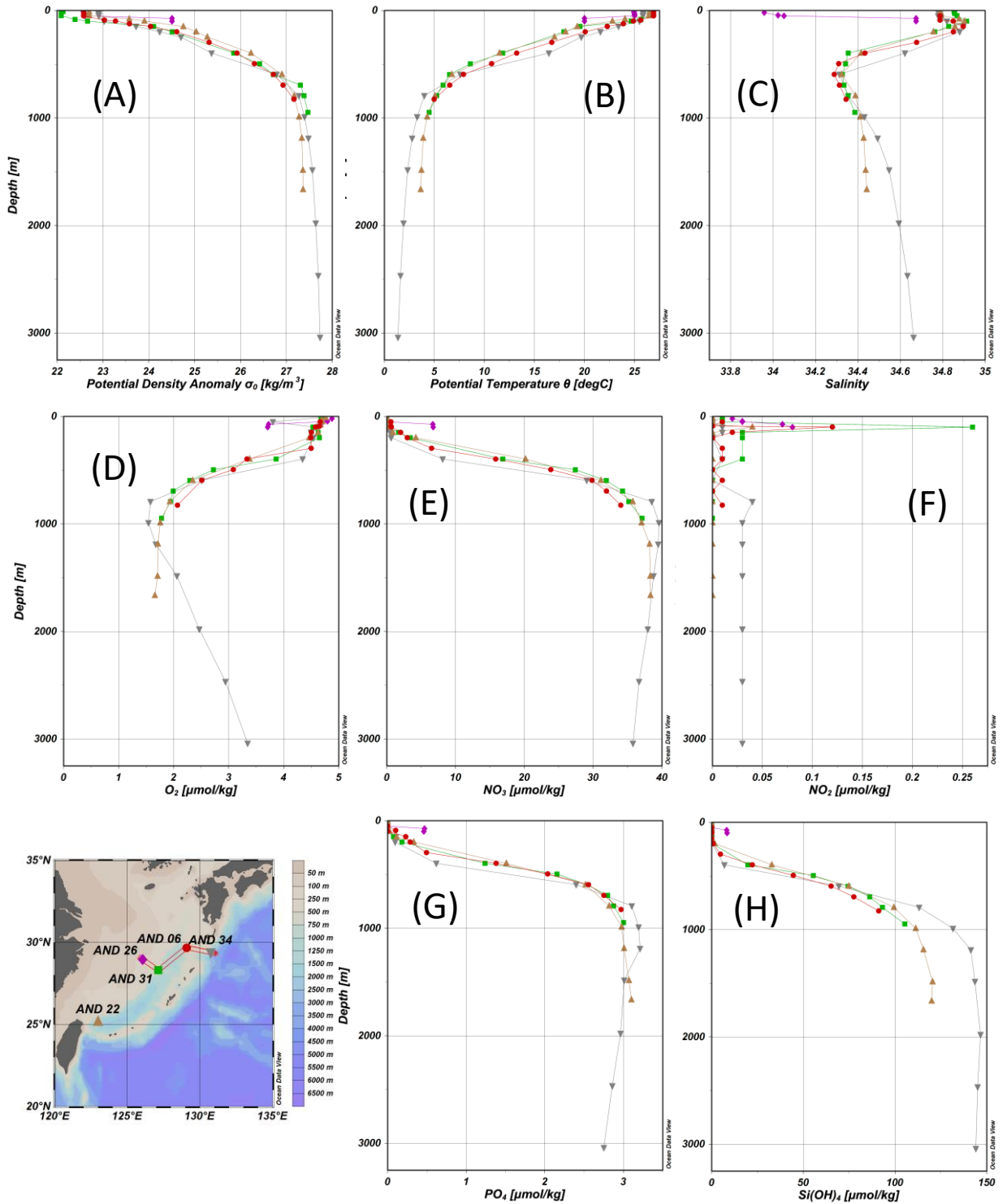


Fig.3 Nakaguchi et al

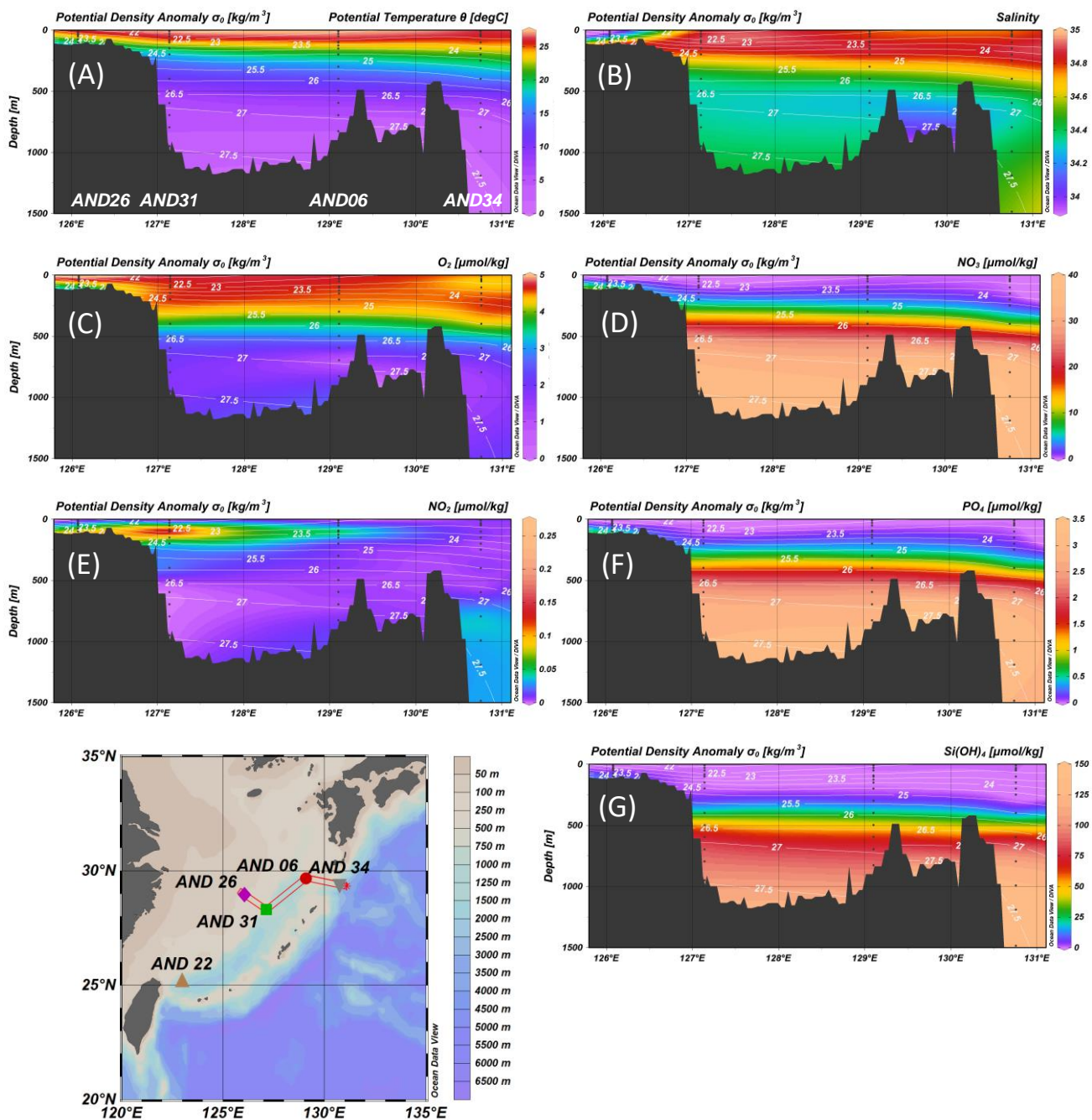


Fig.4 Nakaguchi et al

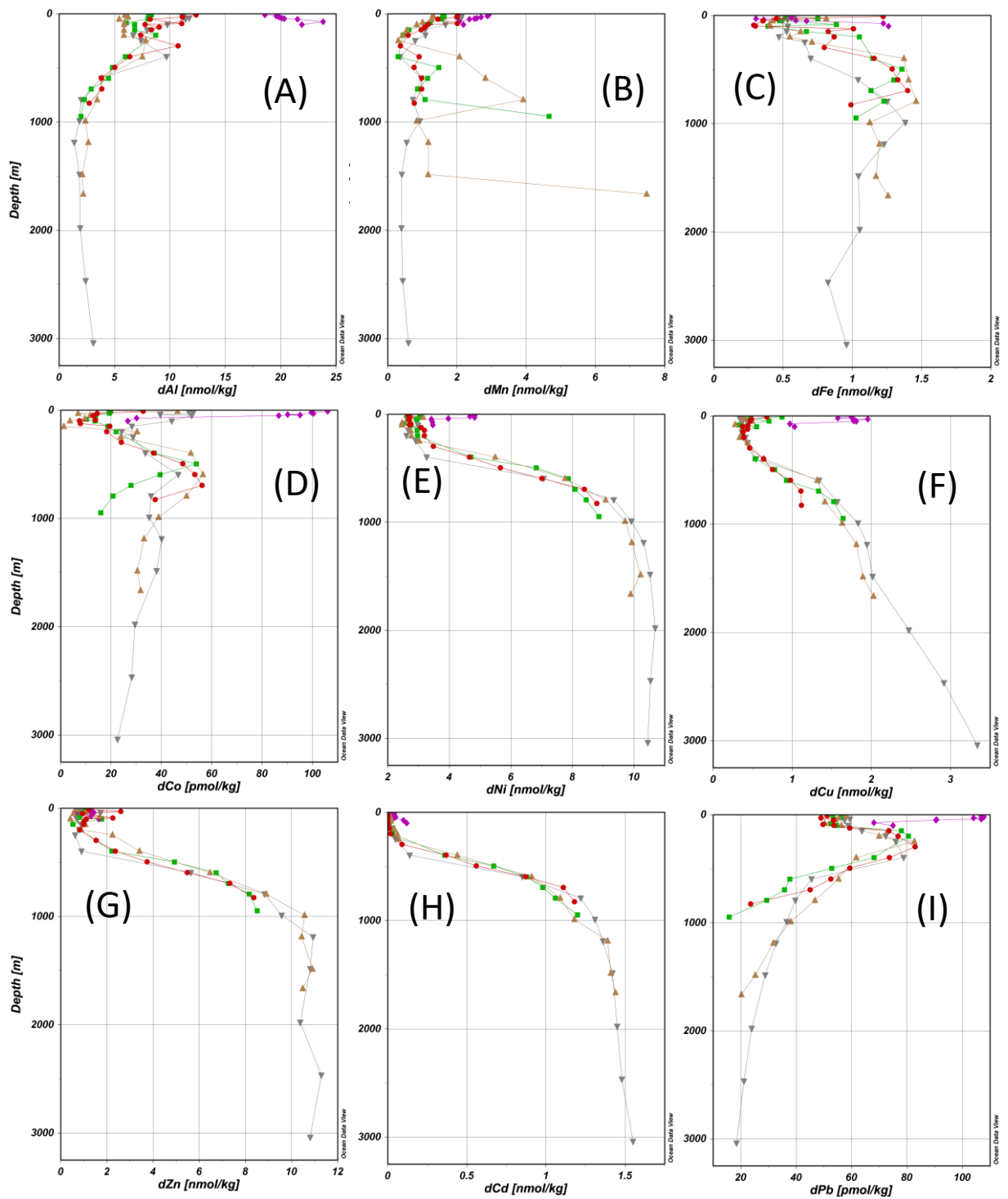


Fig.5 Nakaguchi et al

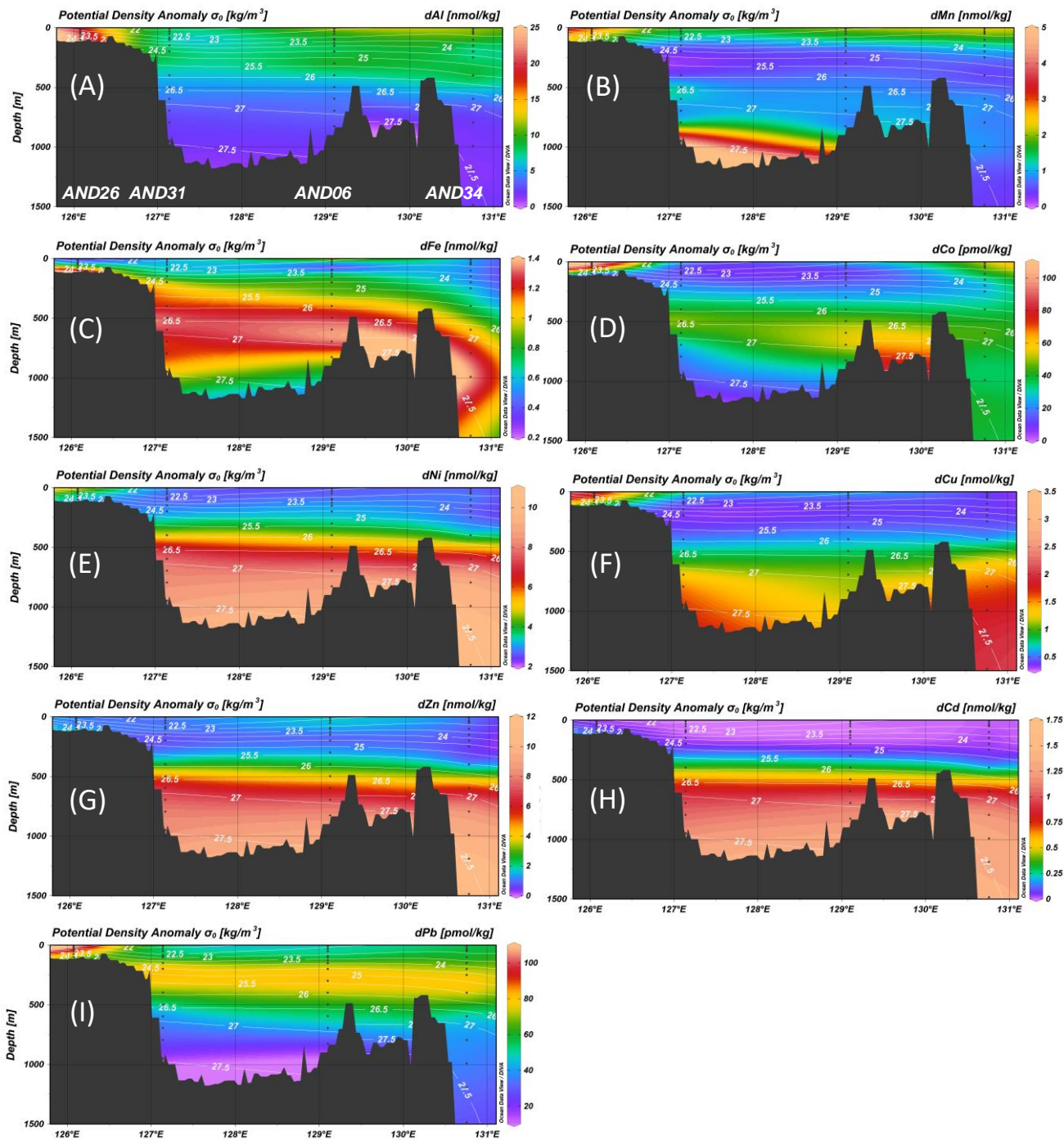


Fig.6 Nakaguchi et al

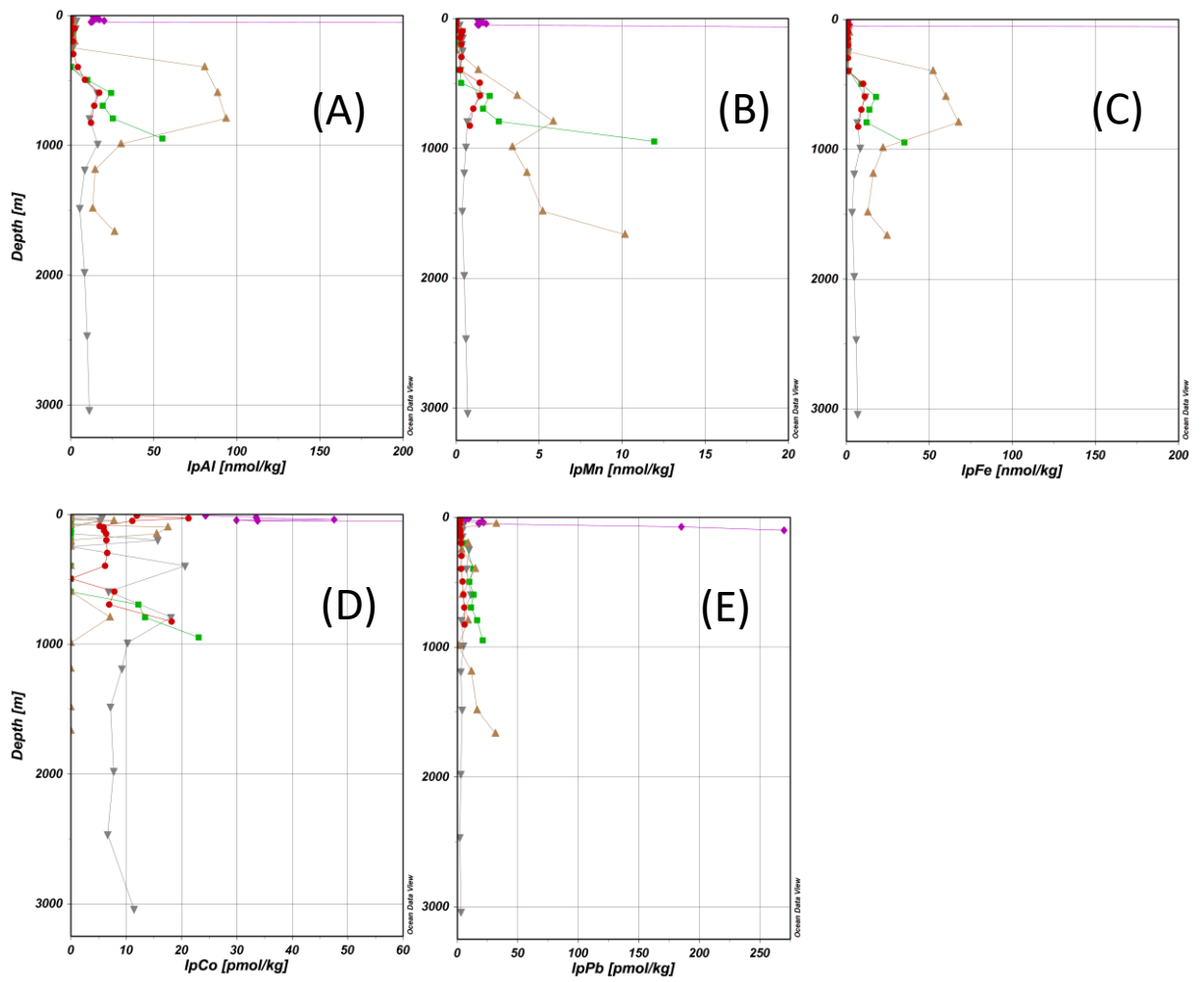


Fig.7 Nakaguchi et al

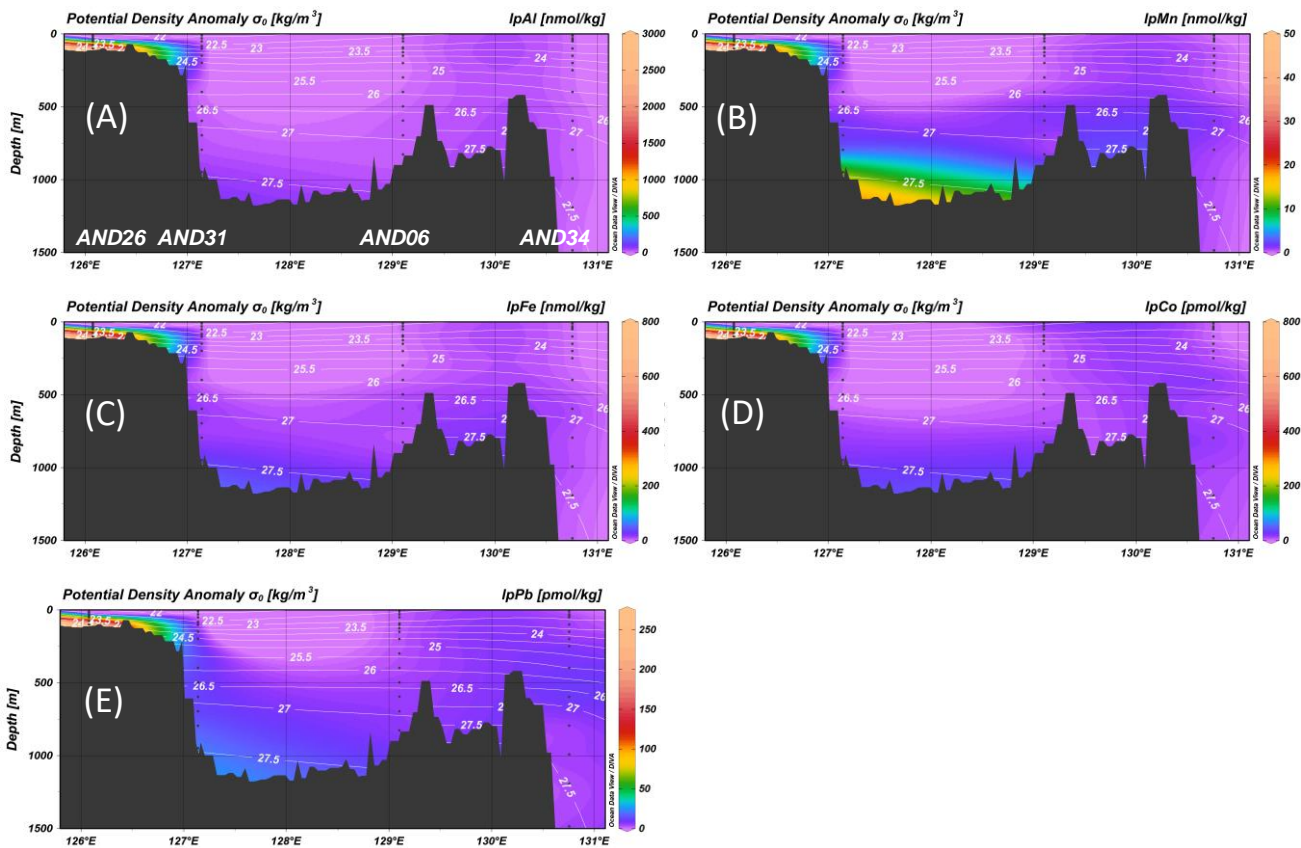


Fig.8 Nakaguchi et al

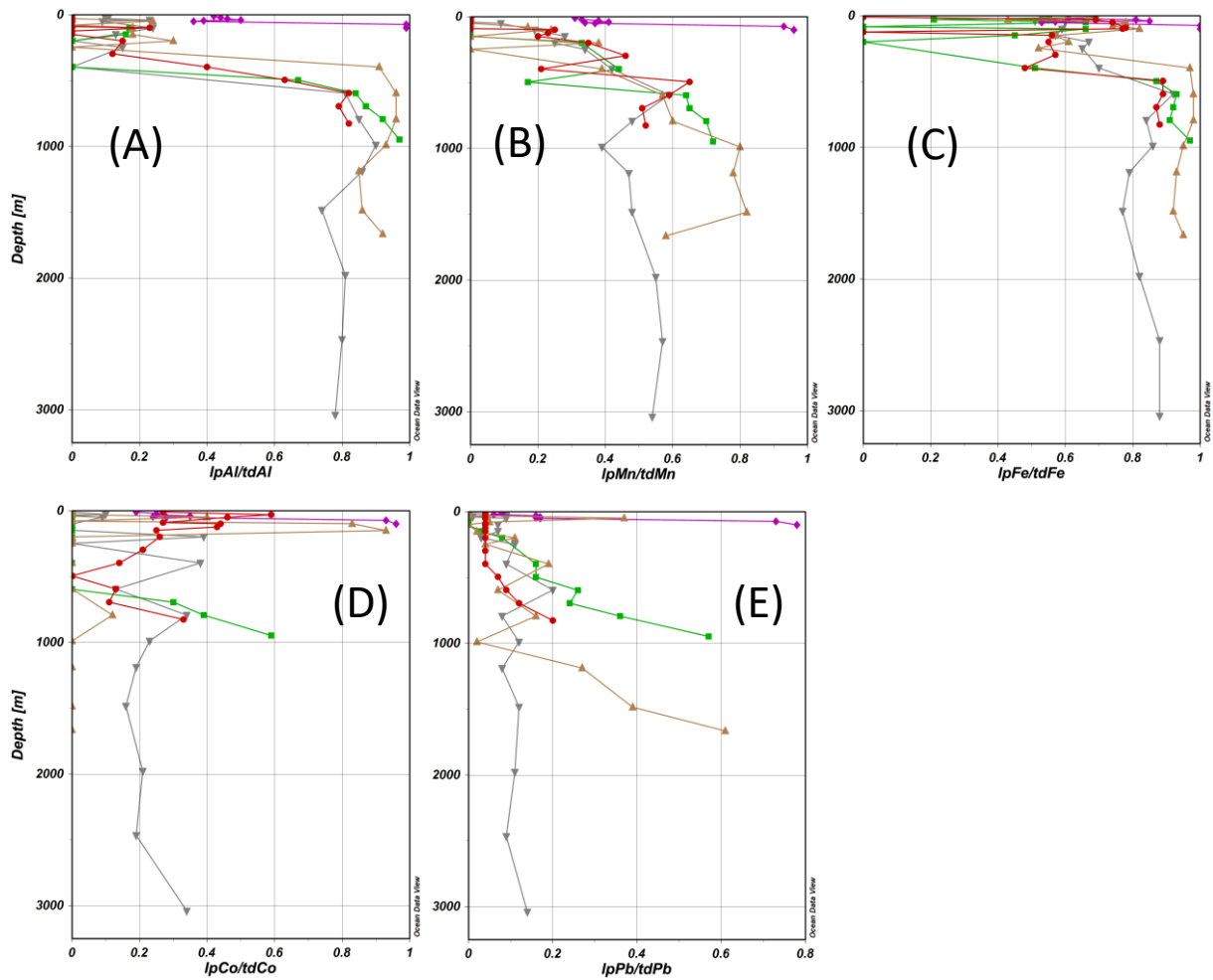


Fig.9 Nakaguchi et al

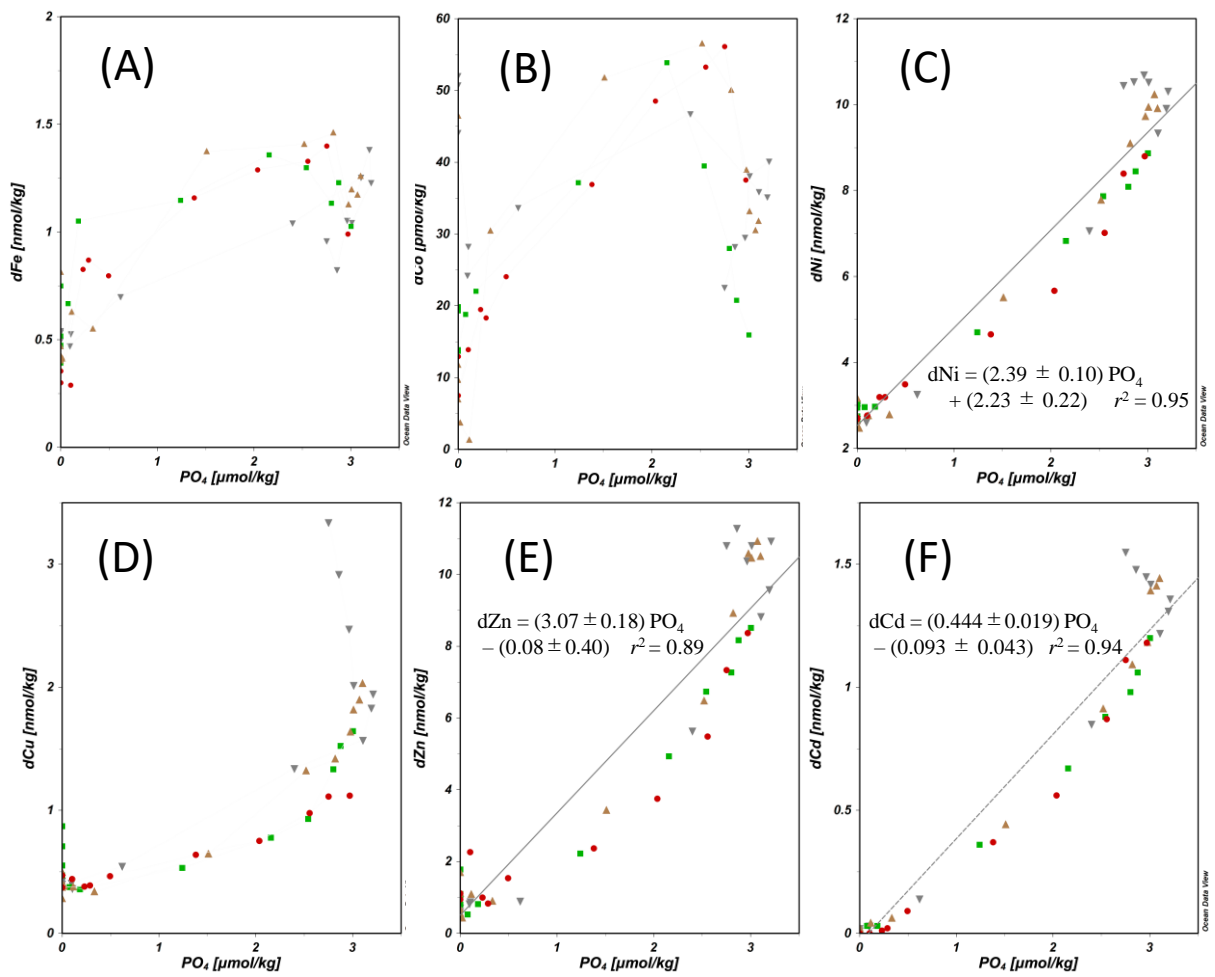


Fig.10 Nakaguchi et al

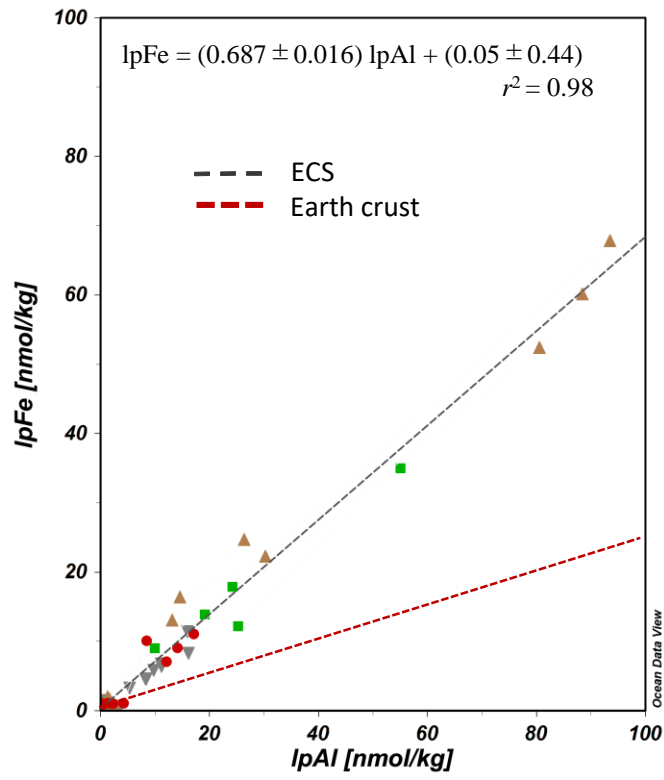


Fig.11 Nakaguchi et al

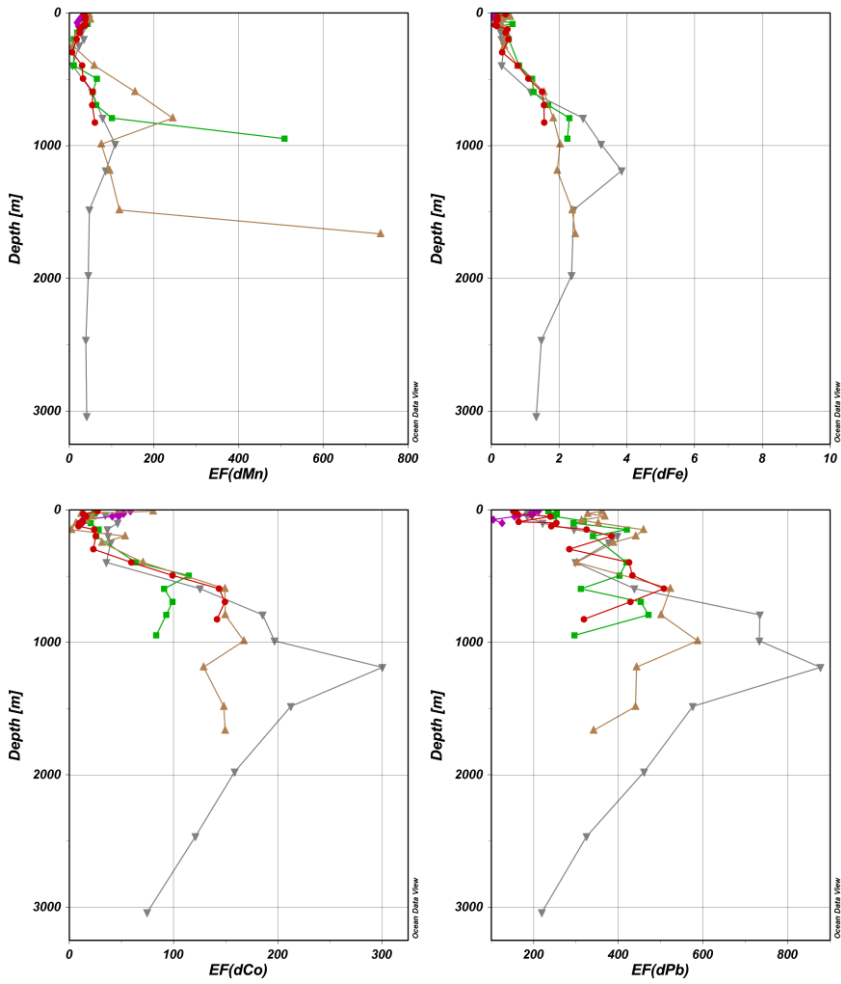


Fig.12 Nakaguchi et al

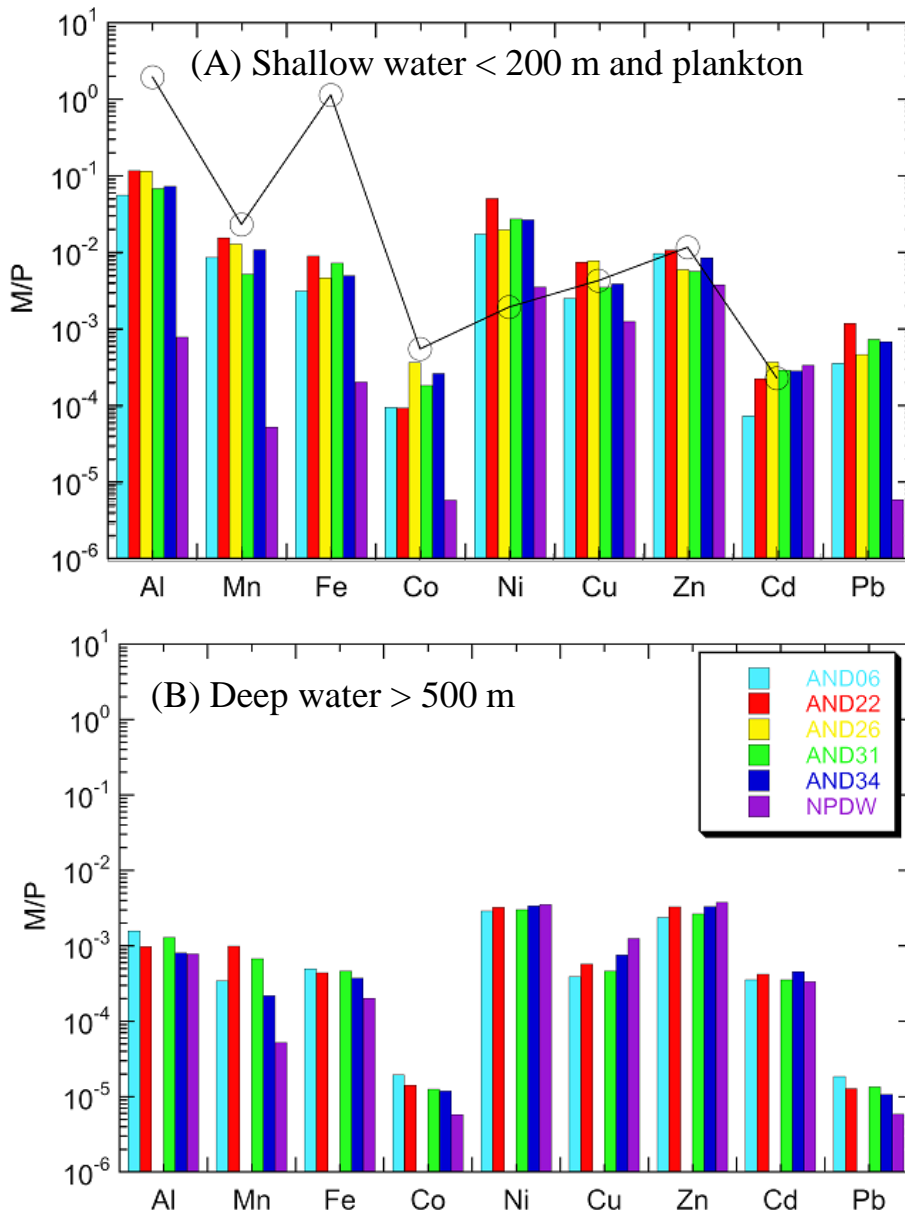


Fig.13 Nakaguchi et al

Table 1 Correlation matrix(r) of nutrients and dissolved trace metals for the pooled data collected in the East China Sea

	Si(OH) ₄	NO ₃	NO ₂	PO ₄	dAl	dMn	dFe	dCo	dNi	dCu	dZn	dCd	dPb
Si(OH) ₄	1.00												
NO ₃	0.95	1.00											
NO ₂	-0.16	-0.26	1.00										
PO ₄	0.94	1.00	-0.27	1.00									
dAl	-0.90	-0.90	0.12	-0.89	1.00								
dMn	0.20	0.21	-0.14	0.26	-0.19	1.00							
dFe	0.29	0.81	-0.38	0.75	-0.62	0.22	1.00						
dCo	0.04	0.61	-0.33	0.51	-0.37	0.10	0.79	1.00					
dNi	0.99	0.98	-0.20	0.97	-0.90	0.22	0.71	0.48	1.00				
dCu	0.92	0.82	-0.08	0.81	-0.79	0.16	0.45	0.23	0.90	1.00			
dZn	0.99	0.96	-0.16	0.95	-0.88	0.24	0.62	0.40	0.99	0.92	1.00		
dCd	0.98	0.98	-0.20	0.97	-0.90	0.24	0.68	0.46	1.00	0.92	0.99	1.00	
dPb	-0.92	-0.79	0.02	-0.86	-0.82	0.32	-0.36	-0.15	-0.86	-0.85	-0.89	-0.88	1.00

Bold values indicate p values less than 0.05

Table 2 The lpM/tdM ratios for Al, Mn, Fe, Co, and Pb in the East China Sea and the North Pacific

Sample	lpAl/tdAl		lpMn/tdMn		lpFe/tdFe		lpCo/tdCo		lpPb/tdPb		
	<i>n</i>	AVE ± SD	<i>n</i>	AVE ± SD	<i>n</i>	AVE ± SD	<i>n</i>	AVE ± SD	<i>n</i>	AVE ± SD	
ECS	All depth	49	0.57 ± 0.32	56	0.41 ± 0.23	63	0.74 ± 0.18	47	0.30 ± 0.23	58	0.15 ± 0.17
	< 400 m	26	0.33 ± 0.26	33	0.30 ± 0.21	40	0.65 ± 0.16	40	0.32 ± 0.27	35	0.12 ± 0.17
	> 400 m	23	0.84 ± 0.09	23	0.58 ± 0.14	23	0.89 ± 0.06	17	0.23 ± 0.14	23	0.20 ± 0.16
North Pacific*	489	0.66 ± 0.31	628	0.24 ± 0.24	625	0.64 ± 0.23	620	0.12 ± 0.18	575	0.02 ± 0.08	

*Zheng et al., 2019; Zheng and Sohrin, 2019

Table 3 Correlation coefficients (r) among libile particulate species

(A) all data

	lpAl	lpMn	lpFe	lpCo	lpPb
lpAl	1.00				
lpMn	0.96	1.00			
lpFe	0.90	0.88	1.00		
lpCo	0.99	0.95	0.89	1.00	
lpPb	0.98	0.97	0.91	0.98	1.00

(B) data except AND26

	lpAl	lpMn	lpFe	lpCo	lpPb
lpAl	1.00				
lpMn	0.35	1.00			
lpFe	0.98	0.43	1.00		
lpCo	0.01	0.03	0.02	1.00	
lpPb	0.08	0.34	0.10	0.00	1.00

Bold values indicate *p* values less than 0.05

Table 4 The enrichment factor of dMs in the East China Sea and the North Pacific

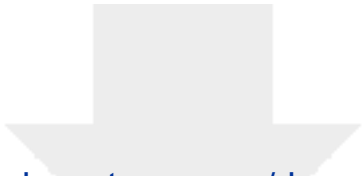
Sample		<i>EF</i> (dMn)		<i>EF</i> (dFe)		<i>EF</i> (dCo)		<i>EF</i> (dNi)	
		<i>n</i>	AVE ± SD	<i>n</i>	AVE ± SD	<i>n</i>	AVE ± SD	<i>n</i>	AVE ± SD
	All depth	67	63 ± 106	67	0.90 ± 0.90	67	71 ± 62	67	(5.4 ± 6.8)×10 ³
ECS	< 400 m	44	30 ± 12	44	0.33 ± 0.19	44	33 ± 19	44	(1.3 ± 0.5)×10 ³
	> 400 m	23	126 ± 165	23	2.0 ± 0.7	23	143 ± 50	23	(1.3 ± 0.6)×10 ⁴
North Pacific*		514	(8.6 ± 13.8)×10 ²	514	9.1 ± 12.2	508	(1.8 ± 2.8)×10 ³	512	(1.1 ± 1.2)×10 ⁵
Sample		<i>EF</i> (dCu)		<i>EF</i> (dZn)		<i>EF</i> (dCd)		<i>EF</i> (dPb)	
		<i>n</i>	AVE ± SD	<i>n</i>	AVE ± SD	<i>n</i>	AVE ± SD	<i>n</i>	AVE ± SD
	All depth	67	(1.8 ± 2.5)×10 ³	67	(3.8 ± 5.7)×10 ³	67	(6.4 ± 9.8)×10 ⁴	67	(3.3 ± 1.4)×10 ²
ECS	< 400 m	44	(4.1 ± 1.4)×10 ²	44	(4.1 ± 2.8)×10 ²	44	(3.5 ± 5.7)×10 ⁴	44	(2.6 ± 0.9)×10 ²
	> 400 m	23	(4.6 ± 2.6)×10 ³	23	(1.0 ± 0.5)×10 ⁴	23	(1.8 ± 0.9)×10 ⁶	23	(4.5 ± 1.5)×10 ²
North Pacific*		511	(4.8 ± 4.7)×10 ⁴	268	(9.3 ± 9.8)×10 ⁴	508	(1.2 ± 1.5)×10 ⁷	489	(6.5 ± 9.1)×10 ³

*Zheng et al., 2019; Zheng and Sohrin, 2019; Zheng et al., submitted


Table 5 Concentrations of dMs and lpMs

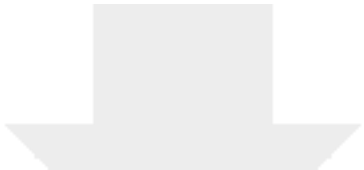
		Offshore Yangtze River*	AND 26	Bering Sea Shelf**
Al (nmol/kg)	d		19–24	2.1–43
	lp		12– 2873	ND–4608
Mn (nmol/kg)	d		2.1–2.9	5.0–23
	lp		1.3–49	1.3–316
Fe (nmol/kg)	d	16.2	0.3–1.3	1.9–19
	lp		0.76– 760	3.8–13187
Co (pmol/kg)	d	940	27–106	140–542
	lp		24–732	23–4471
Ni (nmol/kg)	d		3.4–4.8	4.8–7.5
	lp		ND–2.2	0.89–19
Cu (nmol/kg)	d	22.6	0.98– 2.0	2.2–9.1
	lp		0.28– 1.1	0.34–12
Zn (nmol/kg)	d	14.4	0.60– 1.7	0.8–11
	lp		ND–5.5	0.57–45
Cd (nmol/kg)	d		0.03– 0.12	0.23–0.68
	lp		ND	0.07–0.24
Pb (pmol/kg)	d		65–104	15–91
	lp		ND– 255	3.7–1313

*Su et al., 2017; **Cid et al., 2011




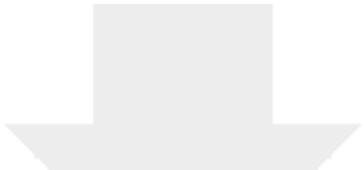
Click here to access/download
Supplementary Material
LOSLC_1_3_Table S1.pdf






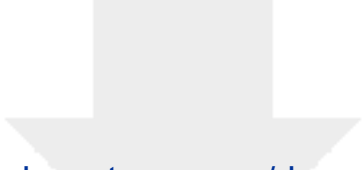
Click here to access/download
Supplementary Material
LOSLC_1_3_Table S2.pdf





Click here to access/download
Supplementary Material
LOSLC_1_3_Table S3.pdf





Click here to access/download
Supplementary Material
LOSLC_1_3_Table S4.pdf

